© 2020. Published by The Company of Biologists Ltd | Development (2020) 147, dev189183. doi:10.1242/dev.189183

RESEARCH ARTICLE

A mutation affecting laminin alpha 5 polymerisation gives rise to a syndromic developmental disorder

Lynelle K. Jones[1,*], Rachel Lam[1,*], Karen K. McKee[2], Maya Aleksandrova[2], John Dowling[3], Stephen I. Alexander[4], Amali Mallawaarachchi[5], Denny L. Cottle[1], Kieran M. Short[1], Lynn Pais[6], Jeffery H. Miner[7], Andrew J. Mallett[8], Cas Simons[9], Hugh McCarthy[10], Peter D. Yurchenco[2] and Ian M. Smyth[1,‡]

ABSTRACT

Laminin alpha 5 (LAMA5) is a member of a large family of proteins that trimerise and then polymerise to form a central component of all basement membranes. Consequently, the protein plays an instrumental role in shaping the normal development of the kidney, skin, neural tube, lung and limb, and many other organs and tissues. Pathogenic mutations in some laminins have been shown to cause a range of largely syndromic conditions affecting the competency of the basement membranes to which they contribute. We report the identification of a mutation in the polymerisation domain of LAMA5 in a patient with a complex syndromic disease characterised by defects in kidney, craniofacial and limb development, and by a range of other congenital defects. Using CRISPR-generated mouse models and biochemical assays, we demonstrate the pathogenicity of this variant, showing that the change results in a failure of the polymerisation of α/β/γ laminin trimers. Comparing these *in vivo* phenotypes with those apparent upon gene deletion in mice provides insights into the specific functional importance of laminin polymerisation during development and tissue homeostasis.

KEY WORDS: Laminin alpha 5, LAMA5, Basement membrane, Kidney, Laminin polymerisation

INTRODUCTION

Basement membranes (BM) are protein-rich sheets which typically separate epithelial or endothelial cells from underlying mesenchyme, thereby mediating the structural integrity of a tissue and communication between cell layers. As a consequence, they are central to normal embryonic development. Laminins constitute a major BM component and are composed of alpha (α), beta (β) and gamma (γ) chains which assemble into 16 different heterotrimeric isoforms (Durbeej, 2010). One of the most broadly and highly expressed of these proteins is laminin alpha 5 (LAMA5) (Miner et al., 1995) which is necessary for normal embryonic development (Miner et al., 1998). By associating with laminin β1, β2, γ1 and γ3, the LAMA5 chain contributes to three major BM trimers: LM-511 (α5/β1/γ1), which is found principally in the BM of epithelia, endothelia and smooth muscle; LM-521 (α5/β2/γ1), which contributes to the BM of epithelia, endothelia, smooth muscle, neuromuscular junctions and the glomerular basement membrane (GBM) of the kidney; and LM-523 (α5/β2/γ3), which has been detected in the retina and CNS. The crucial role that LAMA5 plays in dictating the normal development of these tissues is evident upon its germline inactivation in mice, which results in late gestation embryonic lethality associated with a failure in neural tube closure and placental insufficiency (Miner et al., 1998). In addition, a large number of other developmental defects including syndactyly, defective lung lobation, altered neural crest migration, aborted hair folliculogenesis and abnormal kidney development (amongst others) speak to the breadth of the role of the protein in directing the normal cellular interactions necessary for organogenesis.

LAMA5 is a large (~400 kDa), evolutionarily conserved multidomain protein which forms the central arm of the cruciform structure typical of laminin trimers. The laminin N-terminal domain (LN) present in most other members of the β- and γ-subtypes is associated with polymerisation of laminin hetero-trimers. This process is necessary for the formation of the extensive mesh-like laminin networks that are a feature of BMs (Garbe et al., 2002; Behrens et al., 2012). The laminin complex is linked to (and integrated with) a second major BM protein network composed principally of collagen IV. Early investigations provided evidence that this is mediated through a shared association with nidogen (Fox et al., 1991); however, a more recent study in the skin suggests that perlecan (also known as HSPG2) may also arbitrate these linkages (Behrens et al., 2012). It appears to be likely that such proteoglycan linking is a common feature of BMs generally and that these may be dependent on the tissue in question. The laminin network also interacts extensively with underlying cells in a process mediated in large part through laminin α chains, particularly (though not exclusively) through the engagement of cellular receptors with the laminin globular (LG) domains at their C termini. In the case of LAMA5, potential binding of subsets of the five LG domains (LG1-5) have been identified with integrins α2β1, α3β1, α6β1, α5β4, α7β1 and αvβ3 (Kikkawa et al., 2000; Nishiuchi et al., 2006). In addition, LAMA5 binds to the plasma membrane/membrane-associated proteins α-dystroglycan and syndecan-4 through its LG4

[1]Department of Anatomy and Developmental Biology, Development and Stem Cells Program, Monash Biomedicine Discovery Institute, Monash University, Melbourne 3800, Australia. [2]Department of Pathology and Laboratory Medicine, Robert Wood Johnson Medical School, Rutgers University, Piscataway, NJ 08901, USA. [3]AnatPath, Melbourne 3185, Australia. [4]Nephrology Department, Centre for Kidney Research, The Children's Hospital at Westmead, Sydney 2145, New South Wales, Australia. [5]Department of Medical Genomics, Royal Prince Alfred Hospital; Garvan Institute of Medical Research, Sydney 2010, New South Wales, Australia. [6]Broad Center for Mendelian Genomics, Program in Medical and Population Genetics, Broad Institute of MIT and Harvard, Cambridge, MA 02142, USA. [7]Division of Nephrology, Department of Medicine and Department of Cell Biology and Physiology, Washington University School of Medicine, St Louis, MO 63110, USA. [8]Kidney Health Service, Royal Brisbane and Women's Hospital and the Institute for Molecular Bioscience and Faculty of Medicine, The University of Queensland, Brisbane 4072, Queensland, Australia. [9]Murdoch Children's Research Institute, The Royal Children's Hospital Melbourne, Melbourne 3052, Victoria, Australia. [10]The Sydney Children's Hospitals Network and the Children's Hospital Westmead Clinical School, University of Sydney, Sydney 2145, New South Wales, Australia.
*These authors contributed equally to this work

‡Author for correspondence (ian.smyth@monash.edu)

J.H.M., 0000-0002-1510-8714; C.S., 0000-0003-3147-8042; I.M.S., 0000-0002-1727-7829

Handling Editor: Sally Dunwoodie
Received 17 February 2020; Accepted 30 April 2020

Development (2020) 147, dev189183. doi:10.1242/dev.189183

domain (Nishiuchi et al., 2006; Lin and Kurpakus-Wheater, 2002). Uniquely among α chains, it also binds to basal cell adhesion molecule (BCAM; also known as the Lutheran blood group antigen) (Moulson et al., 2001; Kikkawa et al., 2002).

Many studies of the action of laminins have relied on the use of recombinant proteins, antibody blocking or heterologous *in vitro* expression systems; meaning that the relative contribution of these different interactions to normal embryonic development remain unclear. However, a series of *in vivo* experiments expressing full-length and chimeric LAMA5 in a *Lama5*$^{-/-}$ background explored the specific physiological role of the LG domains (Kikkawa and Miner, 2006). On the basis of these experiments, it appears that LG1-2 harbours much of the functionality involved in embryonic development, as expression of these domains in a fusion transgene with a cDNA encoding LAMA1 LG3-5 rescues the exencephaly, placental vascularisation and lung lobe septation associated with gene deletion. However, these mice still develop progressive renal failure, suggesting that LG3-5 are important for establishing and maintaining the glomerular filtration barrier (Kikkawa and Miner, 2006). Although these findings are important, they may be limited by the universal expression of the transgene employed.

Insights into the functional importance of different laminins have also been provided by the identification of gene mutations in inherited disease. Mutations in *LAMA3*, *LAMB3* or *LAMC2*, which abrogate LM-332 function, cause a skin disorder termed junctional epidermolysis bullosa Herlitz type that is characterised by diminished dermal-epidermal adhesion, skin fragility and blistering (Vidal et al., 1995; Pulkkinen et al., 1994a,b; Aberdam et al., 1994). *LAMA2* loss-of-function mutations cause congenital merosin-deficient muscular dystrophy (MDC1A) (Helbling-Leclerc et al., 1995), whereas hypomorphic missense mutations underpin a milder but related disease limb girdle muscular dystrophy-23 (LGMDR23) (Allamand et al., 1997). Mutations in *LAMB2* give rise to Pierson syndrome, a congenital nephrotic syndrome which rapidly progresses to end-stage renal disease within the first year of life (Zenker et al., 2004). Variants in *LAMB1* are associated with brain malformations known as lissencephaly (Radmanesh et al., 2013) and mutations in *LAMA1* cause cerebellar dysplasia and renal cysts (Aldinger et al., 2014). Despite its broad expression profile and requirement during embryonic development, the evidence for disease-causing mutations in *LAMA5* is less compelling. A homozygous missense variant in domain II of the protein was found in a family with presynaptic congenital myasthenic syndrome (Maselli et al., 2017), but confirmation of causation was not established *in vivo* and interpretation of the patient phenotype was complicated by co-inheritance of a homozygous missense variant in *LAMA1*. Similarly, Sampaolo and colleagues identified heterozygous missense variants in the LAMA5 LG3 domain in a family affected by dominant cutaneous defects and a range of other conditions including variable night blindness, muscle weakness, osteoarthritis, malabsorption syndrome and hypothyroidism (Sampaolo et al., 2017). However, analogous knock-in mice did not display many of these features. Finally, homozygous missense LAMA5 variants (in different protein domains) have been reported in three families with recessive paediatric nephrotic syndrome (Braun et al., 2019) and heterozygous changes in three families with autosomal dominant adult-onset focal segmental glomerulosclerosis (Chatterjee et al., 2013; Gast et al., 2016). However, neither of these studies include functional characterisation to establish whether these variants are causative, correlative or modifiers of the disease phenotypes observed.

Polymerisation is a process which directs the assembly of α/β/γ laminin trimers to form sheet-like networks characteristic of most BMs (Behrens et al., 2012; Garbe et al., 2002). The relative importance of polymerisation to LAMA5 function during fetal development is poorly understood. However, mutations in LAMB2 LN domains cause Pierson syndrome, indicating that abrogated polymerisation is important for maintaining the *in vivo* integrity and functionality of the glomerular BM (McKee et al., 2018; Funk et al., 2018, 2020). Moreover, recent crystallographic studies have identified a protein interface within the LN domain in the region of a PLENGE sequence motif which appears to be important for this oligomerisation (Hussain et al., 2011). In this paper, we report the identification of a compelling disease-causing patient variant in the LN domain of LAMA5 associated with a complex developmental disorder affecting multiple organ systems and reminiscent of the *Lama5*$^{-/-}$ mouse phenotype. This altered residue lies close to the PLENGE sequence thought to be necessary for laminin polymerisation. Using biochemical approaches, we provide evidence that this variant prevents laminin polymerisation. We then employ CRISPR-driven *in vivo* modelling to show that mice carrying the analogous change develop phenotypes which very strongly copy those of the patient. Comparison between the phenotypes of humans and mice with this mutation, and those apparent upon gene deletion, helps to define the functional importance of the LAMA5-LN domain and more broadly of laminin polymerisation to embryonic development.

RESULTS

Clinical data

The proband was the only child to consanguineous healthy parents of Italian descent (Fig. S1) born at 36 weeks of gestation following induced labour, initiated after ultrasound scans indicated advanced polyhydramnios. The pregnancy was also complicated by abnormal nuchal translucency and omphalocoele. Shortly after birth he was diagnosed with 2 large ‘cysts’ in a dysplastic non-functioning right kidney and with bilateral vesicoureteral reflux (VUR) (Fig. 1A). A dimercapto-succinic acid (DMSA) scan in infancy was suggestive of dysplasia in the left kidney. At 2 years he developed atypical focal segmental glomerulosclerosis which was unresponsive to therapy and progressed to end-stage kidney disease and renal transplant shortly afterwards. He then developed a lymphoproliferative disorder 3 years post-transplant, which was thought to be driven by Epstein-Barr virus. In addition, he presented with a complex syndromic condition affecting several other organs. This included short stature and craniofacial dysmorphism (Fig. 1B) including down slanting palpebral fissures, low set dysplastic ears, prominent eyes, micrognathia and mild tongue tie. He also had syndactyly of the 2nd and 3rd toes (Fig. 1C), pyloric web (which was surgically corrected 3 days after birth), atelectasis, undescended testes, bilateral inguinal hernia, absent left vas deferens, and mild and moderate hearing loss in the left and right ears, respectively. He had normal motor and language development and there were no vertebral anomalies.

Panel-based genomic testing for variants in known congenital anomalies of kidney and urinary tract (CAKUT) genes was negative and comparative genomic hybridisation, transferrin isoform profiling and urinary metabolic screening was unremarkable. He was recruited to the KidGen Research Genomics Program (Mallett et al., 2015) and was subjected to whole-genome sequencing (along with his mother), generating mean depth of coverage of 35× and 34×, respectively (with 96% and 93% of bases covered at >20×). Sequence analysis identified a homozygous missense variant

Development (2020) 147, dev189183. doi:10.1242/dev.189183

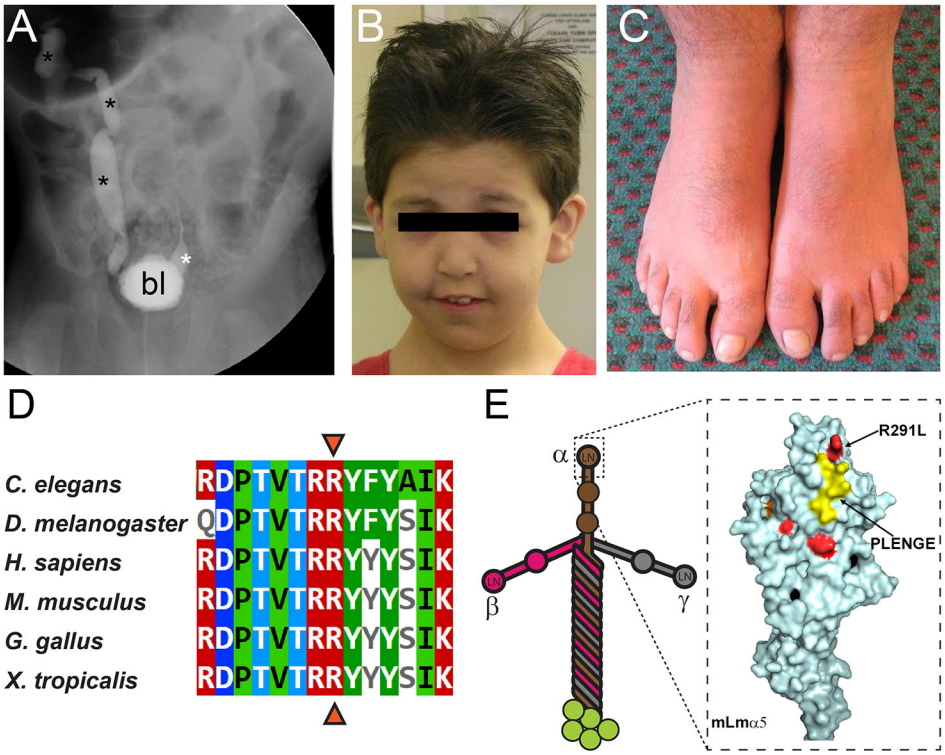

Fig. 1. Identification of a variant in the LN domain of LAMA5 and its impact on polymerisation. (A) Micturating cystourethrogram of the patient at one year of age showing grade 1 reflux on the right kidney (white asterisk) and grade 4 reflux on the left (black asterisks). bl, bladder. (B) Craniofacial malformation in the patient was evident and included down slanting palpebral fissures, low set dysplastic ears, prominent eyes and micrognathia. (C) Syndactyly of the 2nd and 3rd toes. (D) Alignment of LAMA5 orthologues from diverse species (indicated) shows conservation of the arginine residue (291 in mouse). (E) The position of this residue adjacent to the PLENGE domain in the α-chain N-terminal LN domain is indicated on the crystal structure of mouse LAMA5 LN.

[NM_005560.4:c.857G>T; p.(Arg286Leu)] in the LN of LAMA5. This residue is highly conserved across species (Fig. 1D) and, at a structural level, lies adjacent to the PLENGE sequence central to the polymerisation of multiple laminin α/β/γ heterotrimers (Fig. 1E) (Hussain et al., 2011). This variant is not present in the gnomAD database (Lek et al., 2016) and analysis using multiple damage prediction tools (SIFT, Polyphen, LRT, MutationTaster, MutationAssessor, FATHMN, PROVEAN and CADD) consistently predicted the variant as damaging/pathogenic. A summary of further homozygous candidate changes present in the patient is detailed in Table S1.

Laminin polymerisation

The proximity of the variant residue to the PLENGE sequence previously proposed as a mediator of laminin trimer polymerisation (Hussain et al., 2011) raised the possibility that the formation of higher-order laminin networks may be specifically impacted by this alteration. The sequence of the affected residue and those upstream and downstream of this site are highly conserved in laminin α5, α1 and α2 subunits. Because of this, it was possible to study the impact of this change on laminin polymerisation using established protocols for studying this process in chimeric α1 protein. In this approach, a polymerisation-enabling chimeric fusion protein called αLNNd, which comprises the LN domain and a fragment of nidogen (McKee et al., 2018, 2007) can be used in conjunction with full-length γ and β chains and a truncated α chain to model the impact of LN domain variants on polymerisation (Fig. 2A). To this end, we generated wild-type αLNNd protein and a version of the protein carrying the LAMA1 variant equivalent to the LAMA5 mutation (α1R263L). These were then compared to examine whether they could 'rescue' the polymerising capacity of a nidogen-binding LAMA1 construct lacking the LN domain (Lmα1ΔLN-L4b). Laminin assembly was then assayed by the application of recombinant proteins to cultures of Schwann cells, which do not ordinarily generate their own laminin matrix. As expected, wild-type LM-111 was able to contribute to extensive matrix on the surface of these cells, but Lmα1ΔLN-L4b was not (Fig. 2B, upper panels). Although wild-type αLNNd was able to restore matrix assembly with Lmα1ΔLN-L4b, αLNNd bearing the analogous R263L mutation was not (Fig. 2B, lower panels). These findings were confirmed by quantitation of laminin fluorescence (Fig. 2C). The same mutation was also evaluated in a solution-based polymerisation assay with complexes of wild-type or mutated αLNNd+Lmα1ΔLN-L4b. In line with the Schwann cell laminin assembly assay, the incapacity of Lmα1ΔLN-L4b to polymerise (Fig. 2D) was restored by the addition of αLNNd (Fig. 2E) but not by αLNNd bearing the α1R363L substitution (Fig. 2F). These observations were confirmed by quantitation (Fig. 2G). Taken together, this work indicates that the variant in our patient impairs the capacity of LAMA5 to polymerise.

Mouse modelling

To further assess whether the LAMA5 variant in our proband is pathogenic, the change was introduced into the mouse genome using CRISPR-Cas9 genome editing. This was complicated by the fact that the mouse codon analogous to that affected in the patient utilises a different first base (AGG versus CGG). Therefore, the introduction of the same genetic change (G>T) at the second position would result in a different protein alteration (Arg-Met instead of Arg-Leu) (Fig. 3A). Further, the base in question lies near an intron-exon boundary. To address this, we generated two independent mouse lines – a control in which the sequence of the codon was altered to that found in human populations (*Lama5*^{em1Smy}; hereafter *Lama5*^{hs} for 'humanised sequence') and a second in which the genetic change in the proband was introduced to this sequence (*Lama5*^{em2Smy}; hereafter *Lama5*^{pm} for 'point mutation'). This leads to an analogous amino acid change (R291L, Fig. 3A). Transmission of these alleles from founder mice occurred

Development (2020) 147, dev189183. doi:10.1242/dev.189183

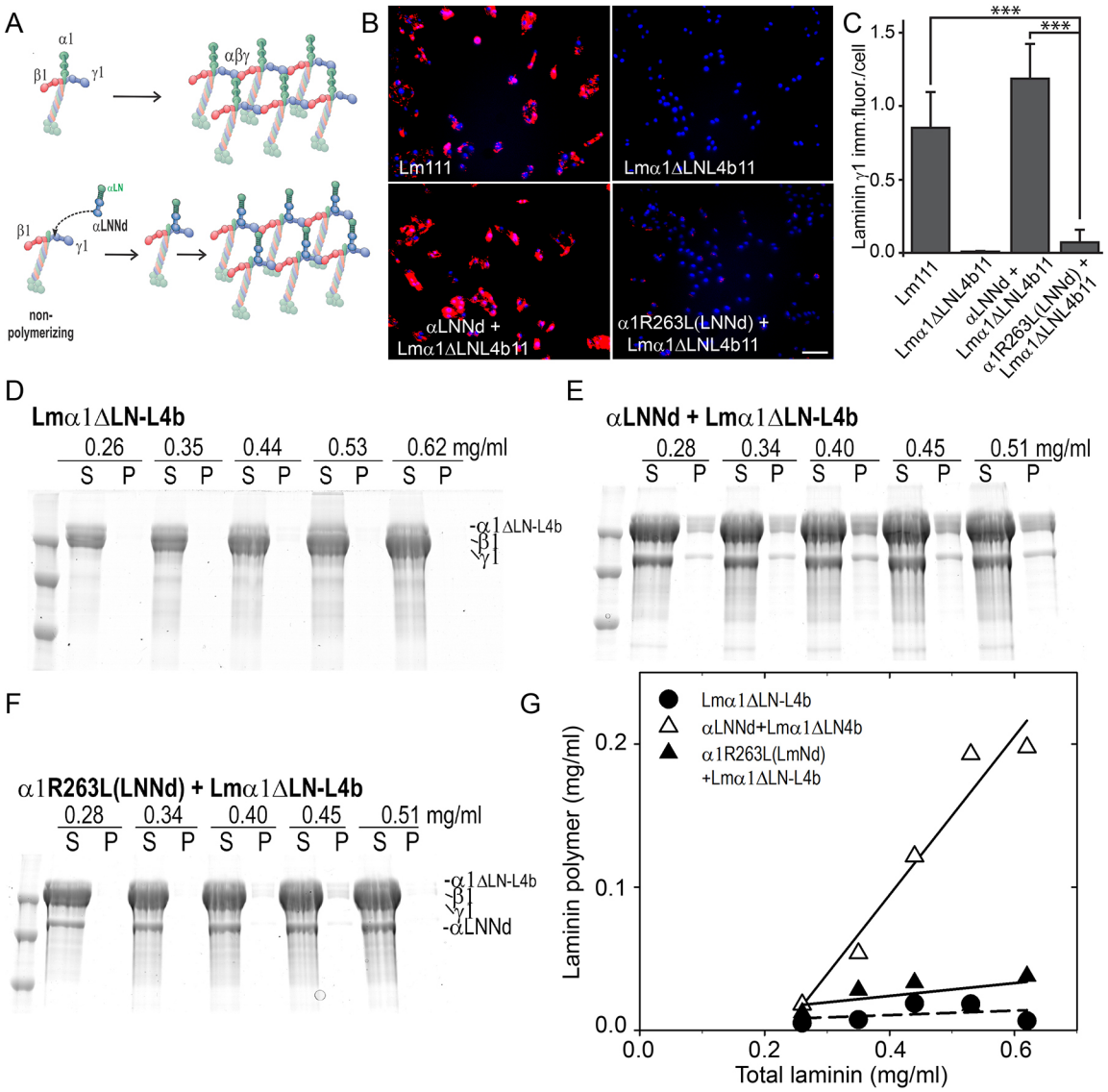

Fig. 2. Evaluation of laminin polymerisation caused by the LN domain variant. (A) Depiction of the experimental system used to assay laminin polymerisation employing a truncated non-polymerising α laminin (Lmα1ΔLN-L4b) and the laminin-nidogen linker protein (αLNNd). The linker protein provides a synthetic arm that binds to the truncated laminin, enabling polymerisation. If the linker protein contains a mutation that inactivates the α1LN domain, the laminin complex is unable to polymerise. (B) Wild-type LM-111, the wild-type and R263L forms of the αLNNd fusion protein and the non-polymerising Lmα1ΔLN-L4b were added to the medium of Schwann cells. Immunostaining for LAMG1 (red) and nuclei (blue) was used to assay for cell-adherent laminin. (C) A plot of the average laminin intensity per cell from the experiment in B (data are mean+s.d., n=7-11 fields/condition, ***$P\leq0.001$, one-way ANOVA). (D-F) SDS-PAGE assay of non-polymerising Lmα1ΔLN-L4b (D) whose function was restored by the addition of the αLNNd fusion (E) but not by the fusion carrying the R263L mutation analogous to that in the patient (F). S, supernatant; P, pellet. (G) Plot of assembly of laminin polymers in samples containing Lmα1ΔLN-L4b alone or with wild-type and mutant αLNNd, demonstrating that the latter does not facilitate laminin polymerisation.

and inter-crosses were established to generate homozygous mice. *Lama5*$^{hs/hs}$ mice were born at Mendelian ratios (n=60, χ^2 P=0.165) and were healthy and fertile. No phenotypes have been noted in these animals in any assay undertaken to date. By contrast, although *Lama5*$^{pm/pm}$ pups were born at the expected ratio (n=7 from 43 pups, χ^2 P=0.073), five were found dead at or shortly after birth, one died at postnatal day (P)15 and the other survived until 4 months of age (P135). Both of the surviving mice were smaller than control littermates (Fig. 3B). Those that died at or around birth had empty stomachs, indicating they had not fed before death. Western blot analysis of extracts from embryonic kidneys at embryonic day (E)18.5 found no difference in the levels of the protein and no evidence of alternate splicing producing smaller forms of the protein (Fig. 3C). Analysis of *Lama5* transcripts in kidney RNA by RT-PCR using primers between exons 4 and 10 found no evidence for alternate splicing caused by either the humanisation of the allele or the introduction of the change at the end of exon 5 (Fig. 3D). Although hair follicle growth and eruption appeared normal in embryos at E18.5 (Fig. 3E), in the two surviving mice there was a significant reduction in fat deposition in the hypodermis, suggestive of wasting (Fig. 3F).

Lama5$^{pm/pm}$ mice display defects in fetal development and growth

Owing to the postnatal mortality observed in the *Lama5*$^{pm/pm}$ mice, we generated cohorts of embryos at E14.5, E16.5 and E18.5 to

Development (2020) 147, dev189183. doi:10.1242/dev.189183

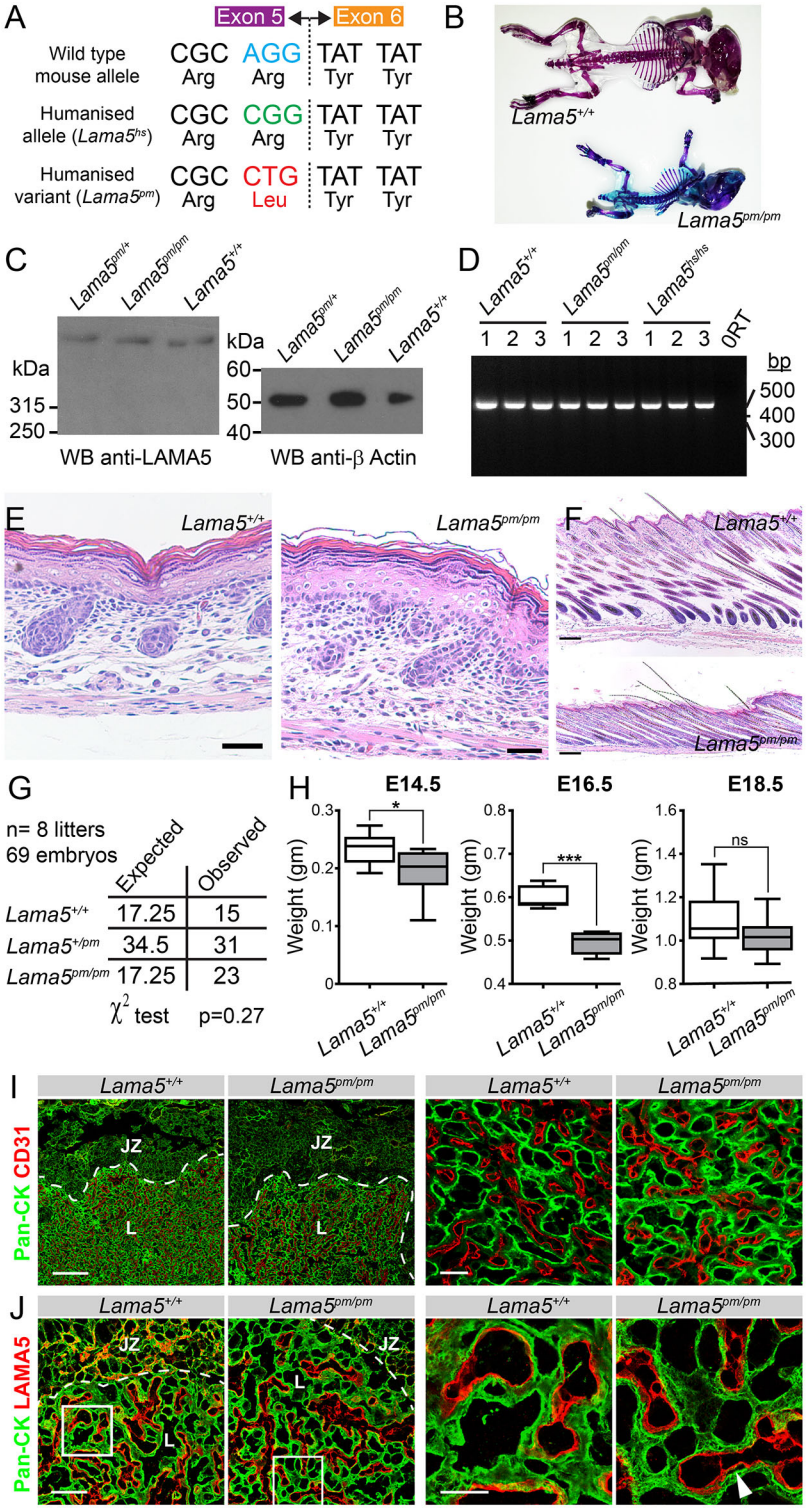

Fig. 3. Identification and modelling of a disease-causing variant in the LAMA5 LN domain. (A) Two different *Lama5* alleles were generated by CRISPR-Cas9 targeting. Note that the different first base in the affected human codon was introduced in the humanised mouse allele (*Lama5*^{hs}) and then mutated to generate the variant allele (*Lama5*^{pm}). (B) The reduction in body size of a surviving P15 *Lama5*$^{pm/pm}$ mouse is illustrated in an Alizarin Red/Alcian Blue skeletal preparation. (C) Western blotting to detect LAMA5 protein in fetal kidney extracts (at E18.5) shows no differences in protein expression or size. A loading control from the same blot using an antibody to β-actin is shown in the right panel. (D) RT-PCR amplification of *Lama5* from exons 4 to 8 from RNA samples isolated from fetal mouse kidneys of the indicated genotypes (at E18.5) shows that splicing in and around the mutation in exon 5 does not result in exon skipping. (E) Skin sections at E18.5 demonstrate normal formation and differentiation of hair follicles; however, a surviving pup at P15 (F) showed an absence of hypodermal adipose tissue, compressing hair follicles against underlying muscle layers. Scale bars: 50 µm in E; 200 µm in F. (G) Inter-crossing of *Lama5*$^{+/pm}$ animals shows no difference between expected and observed embryo genotypes at E18.5. (H) The reduction in weight in mid gestation embryos (E14.5, E16.5) is not observed at E18.5. **P*<0.05, ****P*<0.001; one-way ANOVA with follow up Tukey's multiple comparison test. *n*=9 and 8 for wild type and *Lama5*$^{pm/pm}$, respectively, at E14.5; 5 and 4 at E16.5; 13 and 18 at E18.5. ns, non-significant. (I) Staining for vasculature (CD31) and trophoblasts (pan-cytokeratin) in placenta from *Lama5*$^{pm/pm}$ mice and controls showed no major differences in zonation. Right panels are representative higher magnification of panels on the left. Scale bars: 200 µm in left panels; 25 µm in right panels. (J) Staining for basement membrane (LAMA5) and trophoblasts (pan-cytokeratin) identified small areas of detachment (arrow). Right panels are higher magnification of boxed areas in panels on the left. Scale bars: 50 µm in left panels; 15 µm in right panels. Arrowhead indicates an area of trophoblast detachment. Dashed white lines indicate an area of trophoblast detachment. JZ, junctional zone; LZ, labyrinth zone; Pan-CK, pan-cytokeratin.

examine the impact of the mutation on fetal development. At the latter time point, homozygous embryos were present in the expected Mendelian ratios (χ^2 *P*=0.277, 69 embryos; Fig. 3G), which, combined with postnatal testing, confirms that, unlike *Lama5* knockout mice, *in utero* death is not associated with this variant. Indeed, the exencephaly associated with gene deletion (Miner et al., 1998) was never observed in *Lama5*$^{pm/pm}$ animals. Embryos from *Lama5*$^{pm/pm}$ at E14.5 and E16.5 were smaller than wild-type littermates, but this difference was no longer evident at E18.5 (Fig. 3H), indicating that *in utero* growth restriction was unlikely to contribute to failure to thrive and survive after birth. There was no evidence of sexual dimorphism in the context of survival (χ^2 *P*=0.138) or with respect to embryo weight (*P*=0.395, Welch's *t*-test) at this developmental time point. Germline *Lama5* deletion results in significant failure in the attachment of placental trophoblasts to associated BMs (Miner et al., 1998). On this basis,

Development (2020) 147, dev189183. doi:10.1242/dev.189183

we examined the structure of the placenta of *Lama5*$^{pm/pm}$ in an attempt to identify analogous defects. Immunohistochemical staining for trophoblasts (pan-cytokeratin), endothelial cells (CD31; also known as Pecam1) and basement membrane (LAMA5) revealed no significant differences in the zonation of the placenta in *Lama5*$^{pm/pm}$ mice versus controls (Fig. 3I,J), but did show restricted areas of subtle trophoblast detachment (Fig. 3J). Notably, staining with an anti-LAMA5 antibody was equivalent in both intensity and localisation to wild-type controls, indicating that the variant protein is incorporated into BMs.

Lama5$^{pm/pm}$ mice display gross developmental defects

As was the case with our patient, syndactyly was a fully penetrant phenotype observed in *Lama5*$^{pm/pm}$ mice. In all instances, the forelimbs were more severely affected than hindlimbs and usually had a club-shaped appearance in which individual digits were not delineated (Fig. 4A). Staining of the axial skeleton with Alizarin Red/Alcian Blue found no defects in the underlying patterning of bone and cartilage or fusion of these elements, findings which parallel the soft tissue syndactyly evident in our patient (see Fig. 1C). Comparison of skeletal elements at E16.5 suggested that

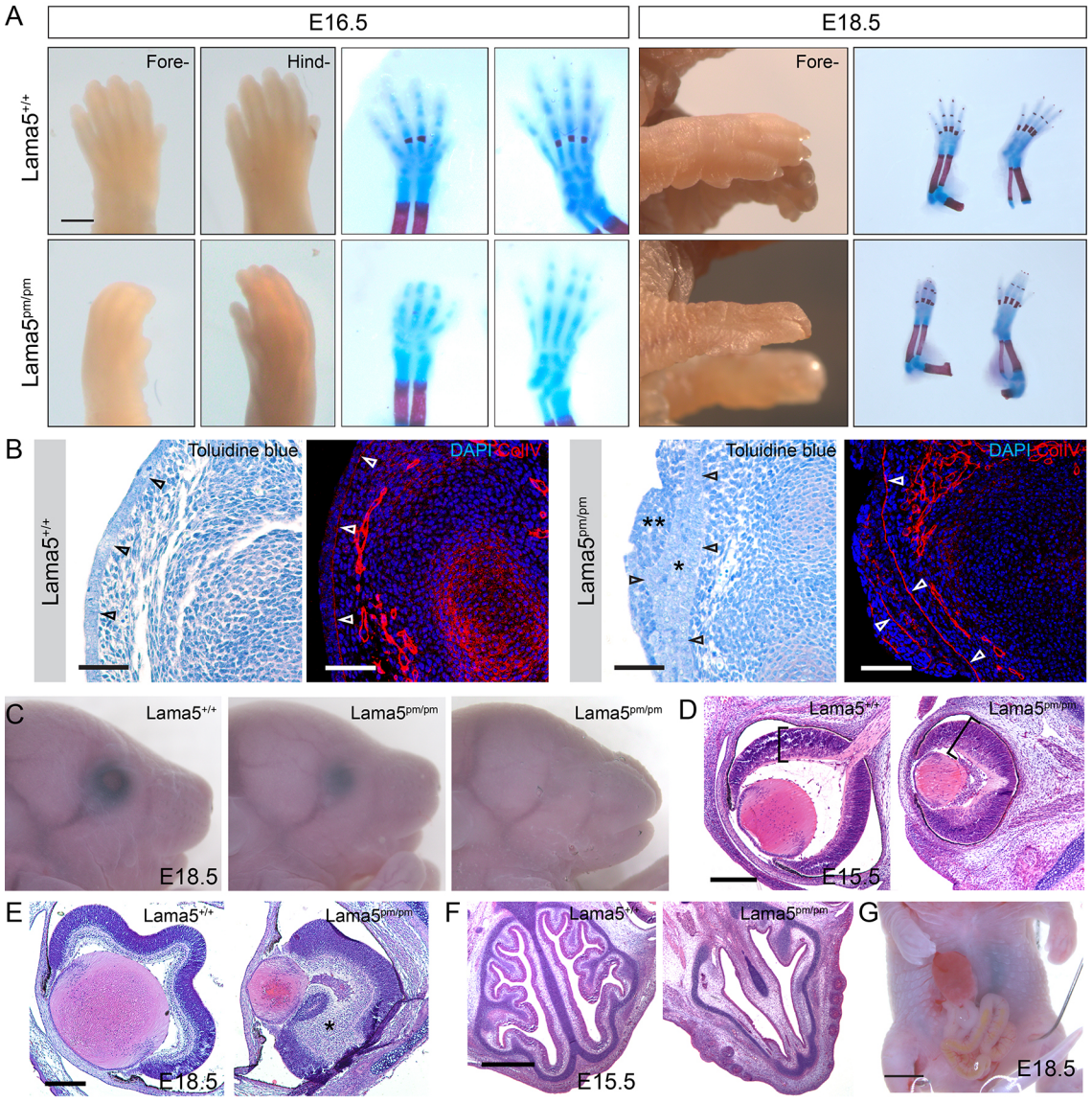

Fig. 4. Gross developmental defects associated with mutation of the LAMA5 LN domain. (A) Soft tissue syndactyly of both fore- and hindlimbs was evident in all *Lama5*$^{pm/pm}$ mice examined, but not in *LAMA5*$^{hs/hs}$ or wild-type controls. Subtle delays in ossification of digit elements observed at E16.5 were not present at E18.5. Panels on the right show staining with Toluidine Blue (blue) and Alizarin Red (red). Scale bar: 500 µm. (B) Histological examination of limb sections at E14.5 shows delineation of epithelia separated from underlying mesenchyme between digits in wild-type mice (black arrowheads, left panel) and the formation of a single, well-defined collagen-rich basement membrane (white arrowheads, right panel). However, in *Lama5*$^{pm/pm}$ embryos extruded mesenchyme (**) that was evident on the apical side of the epithelia (*) (left panel), which was associated on both sides with the formation of basement membrane (right panel; white arrowheads). ColIV, collagen IV. Scale bars: 50 µm in Toluidine-stained sections; 25 µm in immunostained sections. (C) Defects in eye development were evident in some *Lama5*$^{pm/pm}$ embryos at E18.5 and ranged from subtle reductions in size (centre) to anophthalmia (right). (D) Eye sections at E15.5 showed malformation of the normal cupped morphology of the retina as well as a thickening and disorganisation of retinal cell layers (bracketed). Scale bar: 300 µm. (E) At E18.5 such disorganisation was heightened, particularly in cells apical to the outer plexiform layer (asterisk), and extrusion of the lens from the optic cup was occasionally observed. Scale bar: 300 µm. (F) Broader craniofacial defects were also noted, including reduced complexity and trabeculation of the epithelia of the nasal cavity. Scale bar: 1 mm. (G) Infrequent omphalocele was also observed in *Lama5*$^{pm/pm}$ embryos. Scale bar: 2 mm.

Development (2020) 147, dev189183. doi:10.1242/dev.189183

osteogenesis may be delayed as a consequence of the *Lama5* mutation, although these phenotypes were not evident at E18.5 (Fig. 4A). Syndactyly in *Lama5*$^{-/-}$ mice has previously been attributed to a breakdown in inter-phalangeal BM and extrusion of underlying mesenchyme (Miner et al., 1998), and similar defects were observed in *Lama5*$^{pm/pm}$ embryos at E14.5 (Fig. 4B). This analysis also highlighted the development of duplicated BM layers, which were a feature of the knockout mice. Eye abnormalities were recorded in 26% (n=6 of 23) of E18.5 *Lama5*$^{pm/pm}$ mice, manifested unilaterally or bilaterally, were variable in their severity (Fig. 4C) and extended to anophthalmia. In some cases, these were associated with malformation of the frontonasal processes (Fig. 4C, right). Sectioning of skulls at E15.5 (Fig. 4D) and E18.5 (Fig. 4E) revealed malformation of the lens and retina in *Lama5*$^{pm/pm}$ mice, identifying a role for the protein in regulating the normal differentiation of these structures. Craniofacial malformations extended to the nasal cavity and included reduced trabeculation of the nasal epithelia (Fig. 4F). Lastly, omphalocoele was observed in one (4%; n=23) of the E18.5 *Lama5*$^{pm/pm}$ embryos (Fig. 4G), a variably penetrant feature which mirrors the patient phenotype. None of the defects in the limb, face, eye or body wall were observed in *Lama5*$^{+/+}$ littermates (n=28) or *Lama5*$^{hs/hs}$ controls (n=29).

Lama5$^{pm/pm}$ mice display defective lung formation

Our patient presented with recurring atelectasis and *Lama5* knockout mice have been reported to show defects in pulmonary development (Nguyen et al., 2002). To examine whether lung involvement was also a feature of *Lama5*$^{pm/pm}$ mice we examined embryos at E18.5. In wild-type mice, the right lung was always fully septated into the cranial, medial, caudal and accessory lobes (Fig. 5A). However, fusion of the right lung lobes was evident in 27% (n=9 of 33) of *Lama5*$^{pm/pm}$ embryos at E18.5, as was smoothing of the normally defined lobe margins (Fig. 5B). When fusion occurred, the cranial and medial lobes were always affected, although the degree of fusion varied considerably in its extent. There was no evidence of sexual dimorphism in the penetrance of this phenotype (χ^2 P=0.062). Sections of lung showed that fusions were often incomplete, with areas of separation and fusion along the same inter-lobar margin (arrowhead, Fig. 5B). Staining for both LAMA5 and the basement membrane protein collagen IV at E16.5 found that both proteins were still deposited into the BMs of both airways and pleura (Fig. 5C), an observation which differs from those made of *Lama5*$^{-/-}$ mice, which lack a BM at this stage.

Lama5$^{pm/pm}$ mice have abnormal renal development

One of the most prominent clinical features of our patient was the development of multiple defects in renal development and function, some of which appeared functional (focal segmental glomerulosclerosis) and others structural (VUR) in origin. To examine the former, we examined sections of late fetal kidneys but found no gross defects in organ morphology. Immunostaining for collecting ducts and nephron segments also indicated that the development of the organ was relatively normal (Fig. S2). However, upon closer examination of *Lama5*$^{pm/pm}$ kidneys, multiple glomeruli were observed which showed ectatic congested capillaries with fewer vascular profiles than control animals (Fig. 6A). Staining with endothelial (CD31) and podocyte (P57; Coro1a) markers identified a subset of glomeruli that displayed obvious vascular abnormalities, including an enlargement of the vascular space and erosion of the thin vascular walls that create distinct capillaries (Fig. 6A, lower panels). Despite these changes, the cellular organisation of the podocytes around the periphery of the differentiating endothelium/mesangium was indistinguishable from control embryos. These findings are significantly different from the changes observed in *Lama5*$^{-/-}$ mice, in which endothelial and mesangial cells are extruded from the developing glomerulus and the remaining podocytes stratify (Miner and Li, 2000). LAMA5 is thought to contribute significantly to the formation of LM-521 and consequently the integrity of the GBM. Indeed, deletion of the gene results in the absence of this structure (Miner and Li, 2000). To

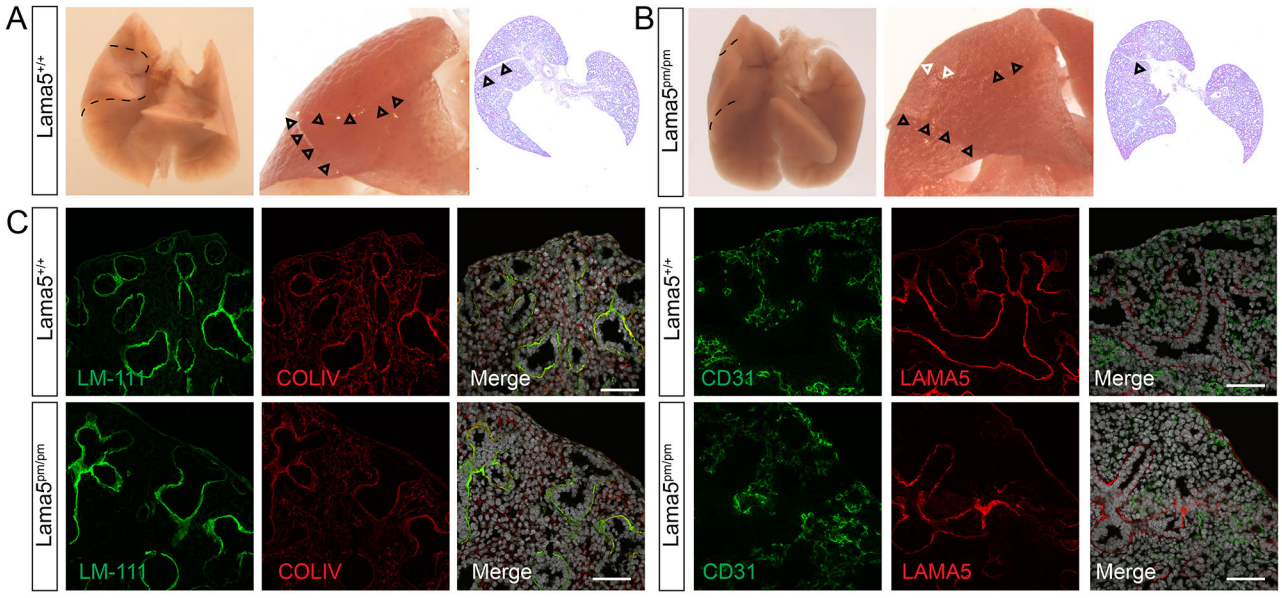

Fig. 5. Lung defects are associated with mutations in the LAMA5 LN domain. (A,B) Lobation and lobar separation of the lung observed in wild-type embryos (dashed lines, black arrowheads) was compromised in a subset of *Lama5*$^{pm/pm}$ embryos which exhibited areas of fusion (white arrowheads). Sectioning showed focal fusions (B, right; arrowhead). (C) Staining with collagen IV (COLIV) and LM-111 demonstrated normal deposition of these proteins into the BM of the airways and lung pleura. Staining with antibodies to CD31 (vasculature) and LAMA5 found no differences in the deposition of these proteins to these BMs. Scale bars: 100 µm.

Development (2020) 147, dev189183. doi:10.1242/dev.189183

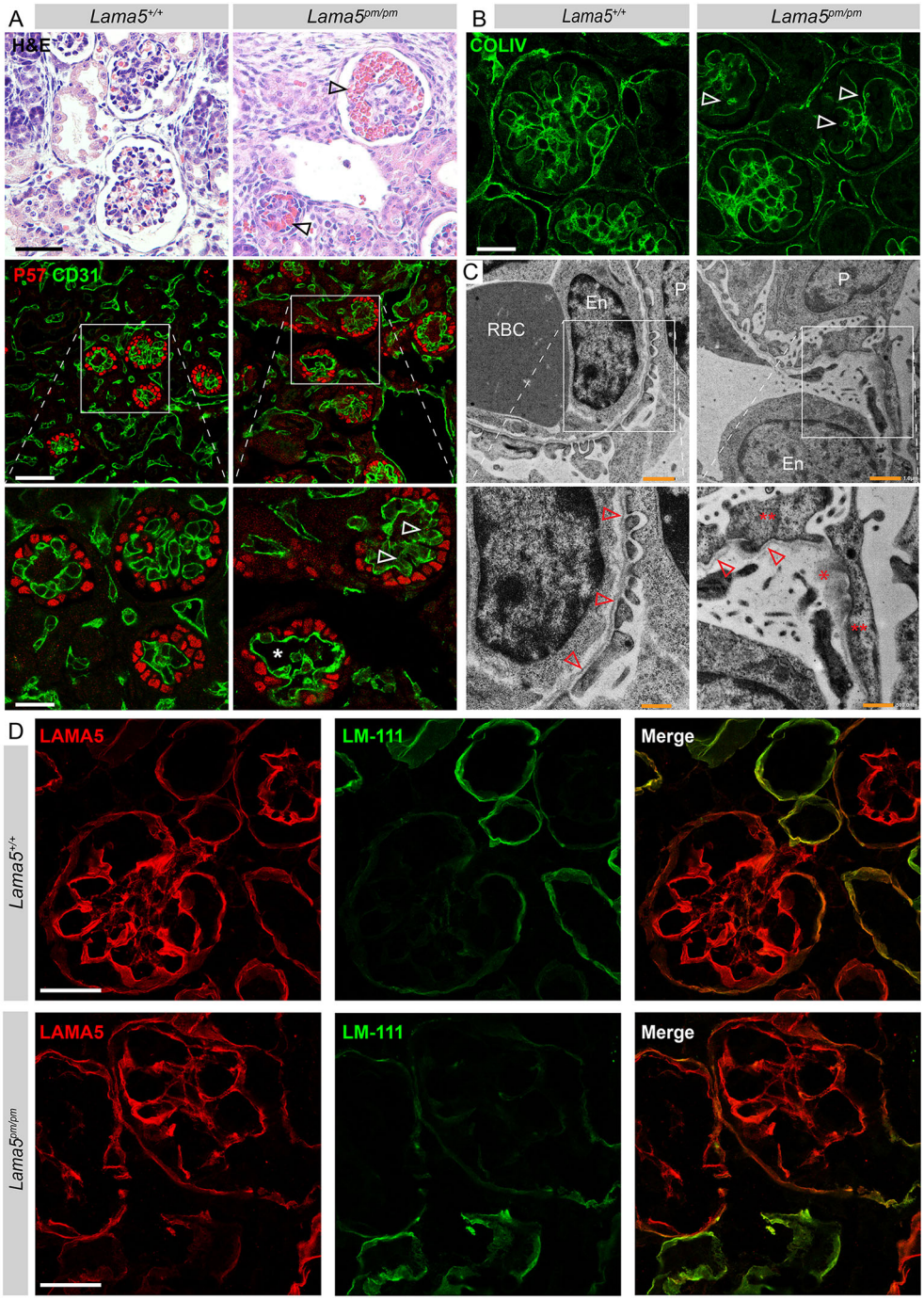

Fig. 6. Glomerular defects in E18.5 *Lama5*$^{pm/pm}$ mice. (A) Late gestation (E18.5) mutant *Lama5*$^{pm/pm}$ fetuses exhibit defects in glomerular structure which are associated with the pooling of erythrocytes (arrowheads; H&E staining, upper panels). These are characterised by alterations in vascular organisation (CD31, immunostaining, middle and lower panels) including large voids (asterisk) and loss of discrete vascular walls (arrowheads). Unlike *Lama5* knockout mice, podocyte organisation in mutant mice is normal, with a single layer of these cells surrounding the vasculature. Lower panels show magnification of boxed areas in middle panels. Scale bars: 50 µm in upper panels; 20 µm in magnifications. (B) Defects in GBM structure at E18.5 are suggested by examination of collagen IV (COLIV) staining, which highlights aggregations of the protein and unusual circular figures (arrowheads) not observed in control animals. Scale bar: 20 µm. (C) Ultrastructure of glomerular capillaries, showing erythrocytes (RBC), endothelial cells (En) and podocytes (P). The GBM formed a uniformly thin and continuous layer in control animals (red arrowheads, left panel), whereas in mutant kidneys the GBM (red arrowheads) was interspersed with areas of disruption to the lamina densa and lamina lucida (*). Podocyte foot processes (**) were dysmorphic compared with the discrete structures present in control animals. Lower panels show magnification of boxed areas in upper panels. Scale bars: 1 µm; 500 nm in magnifications. (D) Immunofluorescent staining showed normal expression and localisation of LAMA5 in *Lama5*$^{pm/pm}$ mice and of LM-111. Merged images confirmed that LAMA5 was present predominantly in the GBM, whereas LM-111 was largely absent from the glomerulus. No compensatory LM-111 overexpression was noted. Scale bars: 20 µm.

investigate whether the LN domain mutation similarly affected the integrity of the GBM, sections were stained with antibodies to collagen IV. This demonstrated that the GBM does form in LAMA5-LN mutant mice but also that some glomeruli had reduced GBM complexity, irregular deposits of the collagen IV protein and constricted vascular profiles not present in the controls (Fig. 6B). To examine these changes in more detail, we performed transmission electron microscopy on kidney sections at E18.5. Compared with the thin, continuous GBMs present in control glomeruli, *Lama5*$^{pm/pm}$ kidneys displayed intermittent areas of disorganisation (Fig. 6C). These alterations in GBM ultrastructure correlated with defective morphology of podocyte foot processes, the broader outlines of which indicate mild effacement compared to the thin and evenly spaced structures present in control embryos (Fig. 6C).

To investigate how mutation of LAMA5 might contribute to these GBM changes we stained sections to determine whether protein deposition was altered. These studies revealed no differences in either the level or localisation of the mutant LAMA5 protein to the GBM (Fig. 6D). Co-staining for LM-111, which is present in early embryonic GBMs and under normal circumstances gradually disappears during embryonic development to be replaced by LAMA5 (Miner and Li, 2000), also detected no significant differences (Fig. 6D). As with our previous studies of LAMA5 deposition in the placenta (Fig. 3J) these studies indicate that LAMA5^{pm} is appropriately translated, transported and

Development (2020) 147, dev189183. doi:10.1242/dev.189183

incorporated into the GBM. The LM-111 staining also indicates that the transition of laminin subtypes in this structure proceeds normally despite the alterations in GBM ultrastructure and vascular differentiation.

Postnatal *Lama5*$^{pm/pm}$ mice develop hydronephrosis

Although the neonatal lethality associated with introduction of the *Lama5*^{pm} mutation limited some investigations of postnatal disease, we were able to study whether other phenotypes emerged in the pups which did survive after birth. At the same time as developing what appeared to be functional glomerular impairment associated with glomerular sclerosis, our patient's renal health was significantly and progressively impaired by VUR. We therefore examined whether the surviving mice at P15 and P135 had evidence of the hydronephrosis typically associated with this condition. Upon dissection, kidneys from both animals exhibited medullary ablation and the formation of voids consistent with the development of this phenotype (Fig. 7A). To confirm that this was caused by hydronephrosis and not by some other mechanism (e.g. the formation of large isolated cysts) we stained sections of kidneys with antibodies to uroplakin IIIa. This protein is expressed in the lining of the renal pelvis, the structure which expands in hydronephrosis. The lining of the voids from these mice stained positive, confirming their origin (Fig. 7B). We also examined the kidneys from surviving mice to determine whether there was evidence of progressive glomerular disease. Surprisingly, given the often-severe phenotypes evident in mutant embryos at E18.5 (see Fig. 6A), the nephrons of these mice were relatively normal, with only occasional vascular malformations noted (Fig. 7C). Variable tubule dilation was observed in the older animals (Fig. 7D) but such phenotypes may be secondary to high grade reflux affecting the animals. The high rate of neonatal death and the poor overall health of these mice precluded more detailed studies of their renal architecture.

DISCUSSION

LAMA5 is one of the most broadly expressed of the laminin subunits during embryonic development but, to date, there is limited evidence for mutations in the gene giving rise to congenital disease. The severity of the phenotypes observed upon germline *Lama5* deletion in mice (Miner et al., 1998) could explain why this might be the case, particularly as exencephaly and placental insufficiency would likely contribute to embryonic death in the event of loss-of-function mutations. However, in the current study we identify a missense mutation in the gene in a patient with a complex syndromic condition whose phenotype correlates with known sites of LAMA5 expression. Analysis of this change in mouse models profiled phenotypes that extensively overlap with those of our

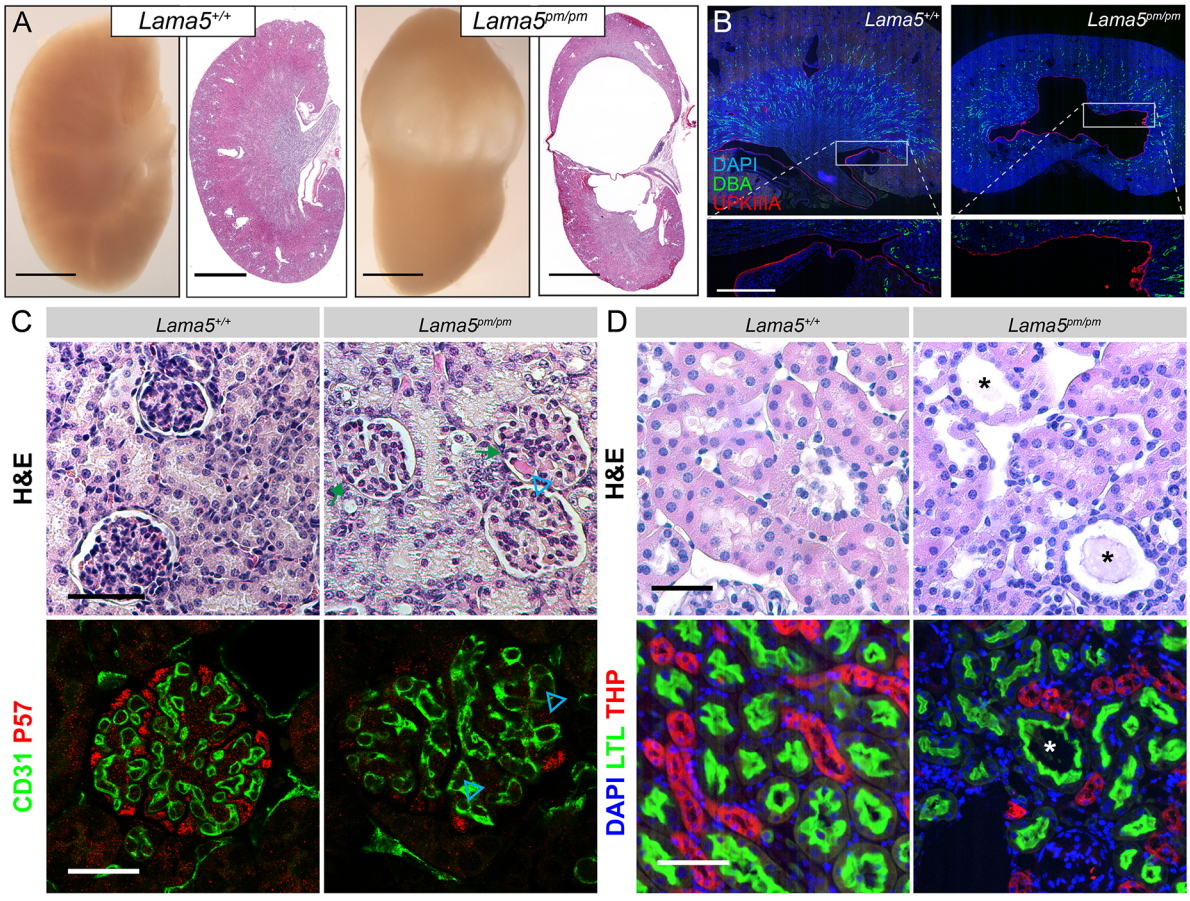

Fig. 7. Postnatal renal defects in *Lama5*$^{pm/pm}$ mice. (A) Hydronephrosis was a feature of those mice which survived past birth. Mutation of *Lama5* resulted in the formation of large voids in the area of the renal pelvis at P135. Scale bars: 2 mm. (B) Staining of sections from affected kidneys showed that the lining of the voids in these organs expressed uroplakin IIIa (UPKIIIA), a marker of the renal pelvis epithelia. Lower panels show magnification of boxed areas in upper panels. Scale bars: 250 µm. (C) Defects in the nephrons at P15 were mild and limited to minor alterations in vascular structure in the glomerulus (blue arrowhead) and some areas of mild sclerosis and adhesion (green arrows). Scale bar: 50 µm in upper panels; 20 µm in lower panels. (D) Defects at P135 were also minor, with some dilation of tubules and protein casts noted (*). Scale bars: 40 µm in upper panels; 70 µm in lower panels.

Development (2020) 147, dev189183. doi:10.1242/dev.189183

patient. These include malformations of the kidney, face, limb, lung and body wall. Importantly, phenotypes such as exencephaly and extensive placental malformation that have been associated with fetal death in *Lama5*$^{-/-}$ mice are absent or ameliorated in our mouse model and in the patient. Taken together with biochemical studies of the variant protein showing that its capacity to polymerise is severely abrogated, this strongly supports the identification of a new syndromic condition specifically associated with hypomorphic mutations in *LAMA5*. Notably though, the mutant LAMA5 protein is normally localised in BMs in multiple tissues. This finding suggests that trimerisation and secretion of the protein is unaffected in our mouse model but also that incorporation of LAMA5 into BM is not wholly dependent on its capacity to form higher order polymerised networks on its own. In this respect, the localisation of laminins and their stable integration into the BM is likely to also be mediated by interactions with a range of cellular and extracellular matrix components including cell-surface receptors, sulphated glycolipids in the cell membrane and through interactions mediated by intermediary proteins such as agrin and nidogen. From our mouse studies it appears that BM integrity is only compromised in tissues which we propose are under greater mechanical stress as a consequence of rapid changes in tissue morphology (limb, lung) or acquisition of function (glomerulus).

Although previous studies of LAMA5 function have focussed on the role of the C-terminal LG domains that are important for engagement with cellular receptors such as integrins, syndecans, dystroglycan and BCAM (reviewed by Spenlé et al., 2013), *in vivo* roles for the LN protein domain are less well understood. The mutation in our patient lies within this part of the protein, adjacent to a sequence considered important for the formation of laminin networks through polymerisation (Hussain et al., 2011). *In vitro* assessment of the LN mutation provides evidence that this change alters the capacity of LAMA5 to polymerise with other LN domains – an essential facet of BM laminin network formation. Consequently, comparing the phenotypes of knockout and *Lama5*$^{pm/pm}$ mice provides an *in vivo* opportunity to assess the function of the LN domain during development. Some aspects of the knockout phenotypes are shared with *Lama5*$^{pm/pm}$ mice, including syndactyly and lung lobe fusion. Both phenotypes have been suggested to arise because of breakdown in BM integrity. In the case of the limb, this is thought to result from the extrusion of underlying digit mesenchyme as a result of a partially competent forming BM (Miner et al., 1998) and in the lung there is evidence that the pleural BM does not form without LAMA5 (Nguyen et al., 2002). Although we observed BM formation in the lung in *Lama5*$^{pm/pm}$ mice, one possibility is that insufficiencies in laminin network formation still result in structural failures of the BM. Notably, the fusion we did observe was variable in its penetrance and often focal in nature. Other phenotypes differ considerably between the two mouse genotypes, including the development of exencephaly, defective hair follicle and tooth morphogenesis, renal agenesis and significant defects in placental vascularisation. All of these features are evident in the knockout mouse but are absent or considerably reduced in *Lama5*$^{pm/pm}$ animals. One interpretation of these results is that engagement with cellular receptors through LAMA5 LG domains and other interacting motifs are still possible in our mutant. Given the normal expression levels and localisation of the LAMA5-PM protein, we propose that such interactions are functionally relevant to the phenotypes which do not develop in *Lama5*$^{pm/pm}$ mice but do develop in knockouts.

Our findings in the kidney represent an example where there exist both phenotypic similarities and differences between knockouts and LN mutants. Germline *Lama5* inactivation results in a failure in GBM formation, an incapacity of the endothelial cells to form capillaries and a failure in podocyte maturation. Introduction of the LN domain mutation leads to very different outcomes. The defects we observed in mutant glomeruli are largely vascular in nature, i.e. the GBM forms but not completely, and the maturation and arrangement of podocytes within the glomerulus are largely normal. In knockout mice the mesangial and endothelial components of the structure are extruded across the course of development, but we do not see similar changes in the LN mutant mice. These findings correlate well with the patient, in whom sclerotic phenotypes parallel the focal breakdown in GBM observed in our mice and with transgenic experiments which suggest that the LG domains still present in our mutant mice are important for glomerulogenesis (Kikkawa and Miner, 2006). The absence of compensatory overexpression of LAMA1, which has previously been observed in *Lama5* knockouts (Goldberg et al., 2010), is not evident. Interestingly the glomeruli of the two *Lama5*$^{pm/pm}$ mice which survived beyond birth were largely normal – with only minor defects in structure. One possibility, given the variability in the appearance of glomerular vascular defects in the *Lama5*$^{pm/pm}$ mice, is that those that are severely affected degenerate as the animals age, but that the aspects of LAMA5 function affected by the mutation are not required for homeostasis after development has ceased.

To the extent that we can tell from the limited number of surviving mice, it appears that changes in the LN domain are not associated with immediate breakdowns in GBM or renal function after birth. However, the extended survival of these mice revealed hydronephrosis as a novel developmental phenotype associated with defects in LAMA5 function and one which may reflect the VUR present in the patient carrying the same mutation. Hydronephrosis can be caused by obstruction of the urinary tract or by urinary reflux associated with changes in the ureter entering the bladder. Although the limited number of surviving *Lama5*$^{pm/pm}$ mice restricted our capacity to assess this functionally, the patient carrying the same variant underwent a micturating cystourethrogram, which showed reflux of urine from the bladder. Given the extensive clinical correlates with our mouse model, this suggests that the development of hydronephrotic phenotypes in LN mutant mice does not arise because of blockage of the urinary tract. However, we cannot definitively exclude the possibility that the same overall phenotype (hydronephrosis) arises through completely different mechanisms.

The hypomorphic nature of the mutation, its proximity to the polymerisation domain of LAMA5 and the specific effect that it has on protein function likely contributes to the rarity of this condition. In general terms it is likely that a proportion of inherited human disease is represented by such 'n=1' families and it may well be that the individual in our study is one of only a handful of people with this type of complex developmental syndrome with causative *LAMA5* mutations. Nevertheless, the evidence that we present to implicate *LAMA5* in disease satisfies the three broad categories outlined by McArthur and colleagues for experimentally investigating causality (MacArthur et al., 2014). Namely, the normal function of LAMA5 in stabilising BMs is consistent with disease aetiology in our patient, the mutation in question functionally disrupts the protein and specifically its capacity to polymerise, and recapitulation of the patient mutation in a model organism results in an analogous phenotype. As such, we feel that studying further rare conditions using CRISPR-based mouse modelling will be clinically and diagnostically valuable. Moreover, our study highlights how such subtle hypomorphic

Development (2020) 147, dev189183. doi:10.1242/dev.189183

changes can provide deeper insights into protein function. In this case they have helped to define the *in vivo* functions of the LAMA5 LN domain and the relative importance of laminin polymerisation in shaping the embryonic development of tissues and organs.

MATERIALS AND METHODS

Patient consent, sequencing and bioinformatic analysis

Human studies were approved as part of the KidGen Research and Functional Genomics project protocols: HREC/14/QRBW/34 and HREC/15/QRCH/126. All participants and their families provided written informed consent for data collection and to undergo clinically relevant genetic/genomic testing. Whole genome sequencing was undertaken on an Illumina X instrument at the Garvan Institute (Australia). Reads were aligned to the reference human genome (GRCh37) using BWA-mem. Single nucleotide variants (SNVs) and indels were called using GATK v3.6 (McKenna et al., 2010), and copy number variants (CNVs) were identified with Canvas and Manta (Roller et al., 2016; Chen et al., 2016). All variants were annotated using SnpEff v3.4 (Cingolani et al., 2012). Analysis and identification of candidate variants were performed with an in-house workflow incorporating the annotated variant data and pedigree information. Parallel analysis was undertaken by Broad Research Genomics. Measures included *in silico* damage prediction (SIFT, Polyphen, LRT, MutationTaster/Assessor, FATHMM, PROVEAN, CADD), assessment of population allele frequencies (gnomAD; Karczewski et al., 2017), read quality analysis and determination of pedigree concordance for all hypothesised inheritance patterns.

Mouse studies

Lama5^{hs} and *Lama5*^{pm} mouse alleles were generated by the Monash Genome Modification Platform (including the Monash University node of the Australian Phenomics Network) by direct injection of CRISPR-Cas9 reagents [guide RNA, recombinant Cas9 protein, HDR repair template (all IDT; 30 ng of each)] into the pronucleus of fertilised mouse oocytes. Mutant alleles were identified in founder mice and backcrossed to wild-type controls for >2 generations before the analysis of any phenotypes. All animals in the study were on a pure C57BL/6J background. Procedures complied with standards set under Australian guidelines for animal welfare and experiments were subject to Monash University animal welfare ethics review (Approval #MARP/2019/13606).

Histology and western blotting

Immunohistochemistry was performed using antibodies to the following proteins: *Dolichos biflorus* agglutinin (DBA) (Vector Laboratories, B-1035, 1:250), *Lotus tetragonolobus* lectin (LTL) (Vector Laboratories, B-1325, 1.250), CD31 (R&D Systems, AF3628, 1:40), cytokeratin (Abcam, Ab11595, 1:100), uroplakin 3a (Progen, 610108, 1:100), collagen IV (Abcam, Ab6586, 1:200), LAMA5 (1:800; Miner et al., 1997), p57 (Santa Cruz Biotechnology, Sc8298, 1:100), Tamm–Horsfall glycoprotein (THP) H-135 (Santa Cruz Biotechnology, Sc20631, 1:100), laminin 111 [gift from Prof. Dale Abrahamson (Abrahamson et al., 1989), 1:1600]. All species-specific Alexa conjugated secondary antibodies were purchased from Invitrogen and used at a dilution of 1:400 [Alexa Fluor Streptavaidin 488, S-11223; Alexa Fluor donkey anti-goat IgG (H+L) 488, A-11055; Alexa Fluor donkey anti-rat IgG (H+L) 488, A-21208; Alexa Fluor donkey anti-rabbit IgG (H+L) 488, A-21206; Alexa Fluor donkey anti-rabbit IgG (H+L) 555, A-31572; and Alexa Fluor donkey anti-mouse IgG (H+L) 555, A-31570]. With the exception of the antisera to LAMA5, all staining was performed on 5 µm paraffin sections following citrate-based antigen retrieval. LAMA5 staining was performed on 10 µm frozen sections of OCT-embedded tissues. Stained sections were mounted in ProLong® Gold Antifade Mountant (Thermo Fisher Scientific) and imaging was performed using a Nikon C1 Upright Confocal microscope. Western blotting was performed using the LAMA5 antibody described above (dilution 1:10,000) and proteins were separated on a precast gradient gel (Bio-Rad). For fetal samples, staining and imaging was performed on a minimum of three different samples from three different animals of each genotype. As indicated, owing to high rates of neonatal death, analysis of surviving *Lama5*$^{pm/pm}$ animals at P15 and P135 was undertaken on limited sample numbers but included $n \geq 3$ for control genotypes.

RT-PCR

RNA from E18.5 snap-frozen kidneys was extracted by crushing organs in RLT buffer using Eppy-pestles and using QiaShredders and RNAeasy minikits (Qiagen) with on-column DNase treatment according to the manufacturer's protocols. cDNA synthesis was performed using Life Technologies VILO on 1 µg RNA. Endpoint PCR was undertaken with 25 ng of cDNA using Green Go Taq mastermix (Promega) with 30 cycles of amplification at 95°C, 30 s at 54°C, 1 min at 72°C. Exon 4 forward primer sequence was 5′-ggggccttgaacttctccta-3′ and exon 8 reverse primer sequence was 5′-gaagaagccaggcagacaac-3′.

Skeletal preparations

Skeletal preparations were performed as per Rigueur and Lyons (2014).

Electron microscopy

After fixation in glutaraldehyde fixative [16% (v/v) paraformaldehyde, 25% (v/v) glutaraldehyde, 0.2 M sodium cacodylate buffer (pH 7.4), 5 mM $CaCl_2$, 10 mM $MgCl_2$] tissues were submitted to the Ramaciotti Centre for Cryo-Electron Microscopy at Clayton for osmication followed by epon resin embedding and sectioning. Imaging was performed using a Jeol 1400Plus microscope.

Recombinant laminins and laminin-nidogen linker proteins

Laminin-111 (LM-111) and non-polymerising laminin lacking the α1 short arm (Lmα1ΔLN-L4b) were prepared and characterised as described previously (McKee et al., 2007). The chimeric linker protein αLNNd was prepared as previously described (McKee et al., 2009). αLNNd bearing the LN domain mutation mouse α1R263L was prepared as follows. Overlapping PCR generated from 1895nt and 290nt products (1F-5′-gactcacggggatttccaagt-3′ and 2R-5′-gccaatagtaataaagtcttgtgacaatggg-3′; 2F-5′-cccattgtcacaagactttattactattcg-3′ and 1R-5′-gatggctggcaactagaaggc-3′) which were sewn together with the 1F and 1R primers. The resulting 2152nt insert was digested with NheI and XhoI (Invitrogen) and ligated with T4 ligase (Invitrogen) into the α1LNNd pcDNA3.1 zeocin vector (ThermoFisher 7648 nt). The α1R263L plasmid was transfected into HEK293 cells and media collected after 5 days of confluent culture. The protein was purified on a flag matrix according to the manufacturer's instructions (Sigma-Aldrich, A2220).

Culturing, immunostaining and analysis of BM assembly in Schwann cells

Schwann cells isolated from sciatic nerves from new-born Sprague-Dawley rats were maintained at high passage, cultured and used to evaluate laminin assembly on cell surfaces as previously described (McKee et al., 2018, 2009). Cells at passage 50 were plated onto 24-well dishes at 50,000 cells/well and treated with the indicated proteins (28 nM laminins, 28 nM αLNNd proteins) for 1 h at 37°C followed by washing, fixation and staining with a primary monoclonal antibody specific for laminin-γ1 as previously described (McKee et al., 2017). Detection of bound primary antibody was accomplished with Alexa Fluor 647 (far red) goat anti-rabbit IgG secondary antibody (A27040, Molecular Probes, 1/400) and nuclear counterstaining with 4′,6-diamidino-2-phenylindole (DAPI). Images were recorded (5-12 fields, each 1300×1030 pixels) using a ×10 objective, with the same exposure time within an experimental set. Fluorescence intensity levels were estimated from the digital images using ImageJ software (National Institutes of Health), with calculations performed in Microsoft Excel. Laminin staining intensities were calculated based on a protocol described for the measurement of laminin on Schwann cells (McKee et al., 2009). Briefly, a single segmentation cut-off value was set to exclude non-cellular regions for all images being compared. The summed pixel intensities overlying the treated cells in each field were then divided by the cell number as determined from DAPI-stained nuclei counts. Values were expressed as the mean±s.d. of summed intensities from different fields normalised to control, with plotting in SigmaPlot 12.5 (Systat Software).

Development (2020) 147, dev189183. doi:10.1242/dev.189183

Laminin polymerisation assay

Aliquots (50 µl) of wild-type LM-111, or Lmα1ΔLN-L4b without or with αLNNd, in polymerisation buffer were incubated at 37°C in a series of concentrations. Eppendorf tubes containing the aliquots were then centrifuged to separate polymerised protein (15,000 ***g***). Supernatants and pellets were analyzed by SDS-PAGE with Coomassie Blue staining, scanned with GE Image Scanner III, and quantitated as previously described (McKee et al., 2009, 2007). Background-subtracted summed pixel values fitted by linear regression were plotted in SigmaPlot 12.5.

Acknowledgements

The studies were performed using the expertise, equipment and reagents of several Monash University Research Platforms including the Monash Genome Modification Platform (incorporating the Australian Phenomics Network), Monash Animal Research Platform, Monash Microimaging, the Ramaciotti Centre for Cryo-Electron Microscopy and the Monash Histology Platform. We are indebted to the patients and families involved and to the clinical, diagnostic and research staff of the KidGen Collaborative. The KidGen Collaborative Flagship is supported by the Melbourne Genomics Health Alliance (Melbourne Genomics), grants from the Royal Children's Hospital Foundation and Royal Brisbane and Women's Hospital Foundation and by the National Health and Medical Research Council Genomics TCR Grant 1113531, entitled 'Preparing Australia for Genomic Medicine: A proposal by the Australian Genomics Health Alliance'. Melbourne Genomics is funded by the 10 members and the State Government of Victoria (Department of Health and Humans Services). In-kind funding support was provided for renal genetics clinic operation and genomic test provision by Queensland Health (Metro North Hospital and Health Service; Children's Health Queensland Hospital and Health Service), New South Wales Health, South Australia Health, Western Australia Department of Health, Northern Territory Department of Health and Tasmanian Department of Health and Human Services. The production of mouse lines in this study were subsidised by the Australian Phenomics Network which is supported by the Australian Government through the National Collaborative Research Infrastructure Strategy (NCRIS) Program. Funding for sequencing was provided by CostCo to the Sydney Children's Hospital Network and the Centre for Kidney Research. The research conducted at the Murdoch Children's Research Institute was supported by the Victorian Government's Operational Infrastructure Support Program. Sequencing and analysis were provided by the Broad Institute of MIT and Harvard Center for Mendelian Genomics (Broad CMG) and was funded by the National Human Genome Research Institute, the National Eye Institute, and the National Heart, Lung and Blood Institute (UM1 HG008900) and in part by the National Human Genome Research Institute grant R01 HG009141.

Competing interests

A.J.M. has received research grant funding from Sanofi-Genzyme and has membership of an Advisory Board for Otsuka, neither of which are related to this project or work.

Author contributions

Conceptualization: R.L., P.D.Y., I.M.S. L.K.J.; Methodology: L.K.J., R.L., J.H.M., P.D.Y., I.M.S.; Formal analysis: L.K.J., R.L., K.K.M., M.A., J.D., C.S., H.M., P.D.Y., I.M.S.; Investigation: L.K.J., R.L., K.K.M., M.A., J.D., S.I.A., A.M., D.L.C., K.M.S., L.P., A.J.M., C.S., H.M., P.D.Y., I.M.S.; Resources: S.I.A., A.M., J.H.M., I.M.S.; Data curation: L.K.J., R.L., K.K.M., M.A., C.S., P.D.Y., I.M.S.; Writing - original draft: R.L., K.K.M., I.M.S.; Writing - review & editing: L.K.J., R.L., K.K.M., M.A., J.D., S.I.A., A.M., D.L.C., K.M.S., L.P., J.H.M., A.J.M., C.S., H.M., P.D.Y., I.M.S.; Visualization: L.K.J., R.L.; Supervision: L.K.J., S.I.A., A.J.M., P.D.Y., I.M.S.; Project administration: S.I.A., A.J.M., H.M., P.D.Y., I.M.S.; Funding acquisition: S.I.A., J.H.M., A.J.M., P.D.Y., I.M.S.

Funding

This work was supported by the National Health and Medical Research Council (APP1098654 to I.M.S., A.J.M., C.S. and S.I.A., APP1106516 to I.M.S.) and the National Institutes of Health (R01-DK36425 to P.D.Y. and R01-DK078314 to J.H.M.). Deposited in PMC for release after 12 months.

Supplementary information

Supplementary information available online at
http://dev.biologists.org/lookup/doi/10.1242/dev.189183.supplemental

Peer review history

The peer review history is available online at
https://dev.biologists.org/lookup/doi/10.1242/dev.189183.reviewer-comments.pdf

References

Aberdam, D., Galliano, M.-F., Vailly, J., Pulkkinen, L., Bonifas, J., Christiano, A. M., Tryggvason, K., Uitto, J., Epstein, E. H., Jr., Ortonne, J.-P. et al. (1994). Herlitz's junctional epidermolysis bullosa is linked to mutations in the gene (LAMC2) for the gamma 2 subunit of nicein/kalinin (LAMININ-5). *Nat. Genet.* **6**, 299-304. doi:10.1038/ng0394-299

Abrahamson, D. R., Irwin, M. H., St John, P. L., Perry, E. W., Accavitti, M. A., Heck, L. W. and Couchman, J. R. (1989). Selective immunoreactivities of kidney basement membranes to monoclonal antibodies against laminin: localization of the end of the long arm and the short arms to discrete microdomains. *J. Cell Biol.* **109**, 3477-3491. doi:10.1083/jcb.109.6.3477

Aldinger, K. A., Mosca, S. J., Tétreault, M., Dempsey, J. C., Ishak, G. E., Hartley, T., Phelps, I. G., Lamont, R. E., O'day, D. R., Basel, D. et al. (2014). Mutations in LAMA1 cause cerebellar dysplasia and cysts with and without retinal dystrophy. *Am. J. Hum. Genet.* **95**, 227-234. doi:10.1016/j.ajhg.2014.07.007

Allamand, V., Sunada, Y., Salih, M. A., Straub, V., Ozo, C. O., Al-Turaiki, M. H., Akbar, M., Kolo, T., Colognato, H., Zhang, X. et al. (1997). Mild congenital muscular dystrophy in two patients with an internally deleted laminin alpha2-chain. *Hum. Mol. Genet.* **6**, 747-752. doi:10.1093/hmg/6.5.747

Behrens, D. T., Villone, D., Koch, M., Brunner, G., Sorokin, L., Robenek, H., Bruckner-Tuderman, L., Bruckner, P. and Hansen, U. (2012). The epidermal basement membrane is a composite of separate laminin- or collagen IV-containing networks connected by aggregated perlecan, but not by nidogens. *J. Biol. Chem.* **287**, 18700-18709. doi:10.1074/jbc.M111.336073

Braun, D. A., Warejko, J. K., Ashraf, S., Tan, W., Daga, A., Schneider, R., Hermle, T., Jobst-Schwan, T., Widmeier, E., Majmundar, A. J. et al. (2019). Genetic variants in the LAMA5 gene in pediatric nephrotic syndrome. *Nephrol. Dial. Transplant.* **34**, 485-493. doi:10.1093/ndt/gfy028

Chatterjee, R., Hoffman, M., Cliften, P., Seshan, S., Liapis, H. and Jain, S. (2013). Targeted exome sequencing integrated with clinicopathological information reveals novel and rare mutations in atypical, suspected and unknown cases of Alport syndrome or proteinuria. *PLoS ONE* **8**, e76360. doi:10.1371/journal.pone.0076360

Chen, X., Schulz-Trieglaff, O., Shaw, R., Barnes, B., Schlesinger, F., Kallberg, M., Cox, A. J., Kruglyak, S. and Saunders, C. T. (2016). Manta: rapid detection of structural variants and indels for germline and cancer sequencing applications. *Bioinformatics* **32**, 1220-1222. doi:10.1093/bioinformatics/btv710

Cingolani, P., Platts, A., Wang Le, L., Coon, M., Nguyen, T., Wang, L., Land, S. J., Lu, X. and Ruden, D. M. (2012). A program for annotating and predicting the effects of single nucleotide polymorphisms, SnpEff: SNPs in the genome of Drosophila melanogaster strain w1118; iso-2; iso-3. *Fly (Austin)* **6**, 80-92. doi:10.4161/fly.19695

Durbeej, M. (2010). Laminins. *Cell Tissue Res.* **339**, 259-268. doi:10.1007/s00441-009-0838-2

Fox, J. W., Mayer, U., Nischt, R., Aumailley, M., Reinhardt, D., Wiedemann, H., Mann, K., Timpl, R., Krieg, T. and Engel, J. (1991). Recombinant nidogen consists of three globular domains and mediates binding of laminin to collagen type IV. *EMBO J.* **10**, 3137-3146. doi:10.1002/j.1460-2075.1991.tb04875.x

Funk, S. D., Bayer, R. H., Malone, A. F., Mckee, K. K., Yurchenco, P. D. and Miner, J. H. (2018). Pathogenicity of a human Laminin beta2 mutation revealed in models of alport syndrome. *J. Am. Soc. Nephrol.* **29**, 949-960. doi:10.1681/ASN.2017090997

Funk, S. D., Bayer, R. H., Mckee, K. K., Okada, K., Nishimune, H., Yurchenco, P. D. and Miner, J. H. (2020). A deletion in the N-terminal polymerizing domain of laminin β2 is a new mouse model of chronic nephrotic syndrome. *Kidney Int.* **29**, 949-960. doi:10.1016/j.kint.2020.01.033

Garbe, J. H. O., Gohring, W., Mann, K., Timpl, R. and Sasaki, T. (2002). Complete sequence, recombinant analysis and binding to laminins and sulphated ligands of the N-terminal domains of laminin alpha3B and alpha5 chains. *Biochem. J.* **362**, 213-221. doi:10.1042/bj3620213

Gast, C., Pengelly, R. J., Lyon, M., Bunyan, D. J., Seaby, E. G., Graham, N., Venkat-Raman, G. and Ennis, S. (2016). Collagen (COL4A) mutations are the most frequent mutations underlying adult focal segmental glomerulosclerosis. *Nephrol. Dial. Transplant.* **31**, 961-970. doi:10.1093/ndt/gfv325

Goldberg, S., Adair-Kirk, T. L., Senior, R. M. and Miner, J. H. (2010). Maintenance of glomerular filtration barrier integrity requires laminin alpha5. *J. Am. Soc. Nephrol.* **21**, 579-586. doi:10.1681/ASN.2009091004

Helbling-Leclerc, A., Zhang, X., Topaloglu, H., Cruaud, C., Tesson, F., Weissenbach, J., Tomé, F. M. S., Schwartz, K., Fardeau, M., Tryggvason, K. et al. (1995). Mutations in the laminin alpha 2-chain gene (LAMA2) cause merosin-deficient congenital muscular dystrophy. *Nat. Genet.* **11**, 216-218. doi:10.1038/ng1095-216

Hussain, S. A., Carafoli, F. and Hohenester, E. (2011). Determinants of laminin polymerization revealed by the structure of the alpha5 chain amino-terminal region. *EMBO Rep.* **12**, 276-282. doi:10.1038/embor.2011.3

Karczewski, K. J., Weisburd, B., Thomas, B., Solomonson, M., Ruderfer, D. M., Kavanagh, D., Hamamsy, T., Lek, M., Samocha, K. E., Cummings, B. B. et al. (2017). The ExAC browser: displaying reference data information from over 60,000 exomes. *Nucleic Acids Res.* **45**, D840-D845. doi:10.1093/nar/gkw971

Kikkawa, Y. and Miner, J. H. (2006). Molecular dissection of laminin alpha 5 in vivo reveals separable domain-specific roles in embryonic development and kidney function. *Dev. Biol.* **296**, 265-277. doi:10.1016/j.ydbio.2006.04.463

Kikkawa, Y., Sanzen, N., Fujiwara, H., Sonnenberg, A. and Sekiguchi, K. (2000). Integrin binding specificity of laminin-10/11: laminin-10/11 are recognized by alpha 3 beta 1, alpha 6 beta 1 and alpha 6 beta 4 integrins. *J. Cell Sci.* **113**, 869-876.

Kikkawa, Y., Moulson, C. L., Virtanen, I. and Miner, J. H. (2002). Identification of the binding site for the Lutheran blood group glycoprotein on laminin alpha 5 through expression of chimeric laminin chains in vivo. *J. Biol. Chem.* **277**, 44864-44869. doi:10.1074/jbc.M208731200

Lek, M., Karczewski, K. J., Minikel, E. V., Samocha, K. E., Banks, E., Fennell, T., O'donnell-Luria, A. H., Ware, J. S., Hill, A. J., Cummings, B. B. et al. (2016). Analysis of protein-coding genetic variation in 60,706 humans. *Nature* **536**, 285-291. doi:10.1038/nature19057

Lin, L. and Kurpakus-Wheater, M. (2002). Laminin alpha5 chain adhesion and signaling in conjunctival epithelial cells. *Invest. Ophthalmol. Vis. Sci.* **43**, 2615-2621.

Macarthur, D. G., Manolio, T. A., Dimmock, D. P., Rehm, H. L., Shendure, J., Abecasis, G. R., Adams, D. R., Altman, R. B., Antonarakis, S. E., Ashley, E. A. et al. (2014). Guidelines for investigating causality of sequence variants in human disease. *Nature* **508**, 469-476. doi:10.1038/nature13127

Mallett, A., Patel, C., Maier, B., Mcgaughran, J., Gabbett, M., Takasato, M., Cameron, A., Trnka, P., Alexander, S. I., Rangan, G. et al. (2015). A protocol for the identification and validation of novel genetic causes of kidney disease. *BMC Nephrol.* **16**, 152. doi:10.1186/s12882-015-0148-8

Maselli, R. A., Arredondo, J., Vázquez, J., Chong, J. X., University of Washington center for Mendelian Genomics, Bamshad, M. J., Nickerson, D. A., Lara, M., Ng, F., Lo, V. L. et al. (2017). Presynaptic congenital myasthenic syndrome with a homozygous sequence variant in LAMA5 combines myopia, facial tics, and failure of neuromuscular transmission. *Am. J. Med. Genet. A* **173**, 2240-2245. doi:10.1002/ajmg.a.38291

Mckee, K. K., Harrison, D., Capizzi, S. and Yurchenco, P. D. (2007). Role of laminin terminal globular domains in basement membrane assembly. *J. Biol. Chem.* **282**, 21437-21447. doi:10.1074/jbc.M702963200

Mckee, K. K., Capizzi, S. and Yurchenco, P. D. (2009). Scaffold-forming and adhesive contributions of synthetic Laminin-binding proteins to basement membrane assembly. *J. Biol. Chem.* **284**, 8984-8994. doi:10.1074/jbc.M809719200

Mckee, K. K., Crosson, S. C., Meinen, S., Reinhard, J. R., Rüegg, M. A. and Yurchenco, P. D. (2017). Chimeric protein repair of laminin polymerization ameliorates muscular dystrophy phenotype. *J. Clin. Invest.* **127**, 1075-1089. doi:10.1172/JCI90854

Mckee, K. K., Aleksandrova, M. and Yurchenco, P. D. (2018). Chimeric protein identification of dystrophic, Pierson and other laminin polymerization residues. *Matrix Biol.* **67**, 32-46. doi:10.1016/j.matbio.2018.01.012

Mckenna, A., Hanna, M., Banks, E., Sivachenko, A., Cibulskis, K., Kernytsky, A., Garimella, K., Altshuler, D., Gabriel, S., Daly, M. et al. (2010). The genome analysis toolkit: a MapReduce framework for analyzing next-generation DNA sequencing data. *Genome Res.* **20**, 1297-1303. doi:10.1101/gr.107524.110

Miner, J. H. and Li, C. (2000). Defective glomerulogenesis in the absence of laminin alpha5 demonstrates a developmental role for the kidney glomerular basement membrane. *Dev. Biol.* **217**, 278-289. doi:10.1006/dbio.1999.9546

Miner, J. H., Lewis, R. M. and Sanes, J. R. (1995). Molecular cloning of a novel laminin chain, alpha 5, and widespread expression in adult mouse tissues. *J. Biol. Chem.* **270**, 28523-28526. doi:10.1074/jbc.270.48.28523

Miner, J. H., Patton, B. L., Lentz, S. I., Gilbert, D. J., Snider, W. D., Jenkins, N. A., Copeland, N. G. and Sanes, J. R. (1997). The laminin alpha chains: expression, developmental transitions, and chromosomal locations of alpha1-5, identification of heterotrimeric laminins 8-11, and cloning of a novel alpha3 isoform. *J. Cell Biol.* **137**, 685-701. doi:10.1083/jcb.137.3.685

Miner, J. H., Cunningham, J. and Sanes, J. R. (1998). Roles for laminin in embryogenesis: exencephaly, syndactyly, and placentopathy in mice lacking the laminin alpha5 chain. *J. Cell Biol.* **143**, 1713-1723. doi:10.1083/jcb.143.6.1713

Moulson, C. L., Li, C. and Miner, J. H. (2001). Localization of Lutheran, a novel laminin receptor, in normal, knockout, and transgenic mice suggests an interaction with laminin alpha5 in vivo. *Dev. Dyn.* **222**, 101-114. doi:10.1002/dvdy.1169

Nguyen, N. M., Miner, J. H., Pierce, R. A. and Senior, R. M. (2002). Laminin alpha 5 is required for lobar septation and visceral pleural basement membrane formation in the developing mouse lung. *Dev. Biol.* **246**, 231-244. doi:10.1006/dbio.2002.0658

Nishiuchi, R., Takagi, J., Hayashi, M., Ido, H., Yagi, Y., Sanzen, N., Tsuji, T., Yamada, M. and Sekiguchi, K. (2006). Ligand-binding specificities of laminin-binding integrins: a comprehensive survey of laminin-integrin interactions using recombinant alpha3beta1, alpha6beta1, alpha7beta1 and alpha6beta4 integrins. *Matrix Biol.* **25**, 189-197. doi:10.1016/j.matbio.2005.12.001

Pulkkinen, L., Christiano, A. M., Airenne, T., Haakana, H., Tryggvason, K. and Uitto, J. (1994a). Mutations in the gamma 2 chain gene (LAMC2) of kalinin/laminin 5 in the junctional forms of epidermolysis bullosa. *Nat. Genet.* **6**, 293-297. doi:10.1038/ng0394-293

Pulkkinen, L., Christiano, A. M., Gerecke, D., Wagman, D. W., Burgeson, R. E., Pittelkow, M. R. and Uitto, J. (1994b). A homozygous nonsense mutation in the beta 3 chain gene of laminin 5 (LAMB3) in Herlitz junctional epidermolysis bullosa. *Genomics* **24**, 357-360. doi:10.1006/geno.1994.1627

Radmanesh, F., Caglayan, A. O., Silhavy, J. L., Yilmaz, C., Cantagrel, V., Omar, T., Rosti, B., Kaymakcalan, H., Gabriel, S., Li, M. et al. (2013). Mutations in LAMB1 cause cobblestone brain malformation without muscular or ocular abnormalities. *Am. J. Hum. Genet.* **92**, 468-474. doi:10.1016/j.ajhg.2013.02.005

Rigueur, D. and Lyons, K. M. (2014). Whole-mount skeletal staining. *Methods Mol. Biol.* **1130**, 113-121. doi:10.1007/978-1-62703-989-5_9

Roller, E., Ivakhno, S., Lee, S., Royce, T. and Tanner, S. (2016). Canvas: versatile and scalable detection of copy number variants. *Bioinformatics* **32**, 2375-2377. doi:10.1093/bioinformatics/btw163

Sampaolo, S., Napolitano, F., Tirozzi, A., Reccia, M. G., Lombardi, L., Farina, O., Barra, A., Cirillo, F., Melone, M. A. B., Gianfrancesco, F. et al. (2017). Identification of the first dominant mutation of LAMA5 gene causing a complex multisystem syndrome due to dysfunction of the extracellular matrix. *J. Med. Genet.* **54**, 710-720. doi:10.1136/jmedgenet-2017-104555

Spenlé, C., Simon-Assmann, P., Orend, G. and Miner, J. H. (2013). Laminin alpha5 guides tissue patterning and organogenesis. *Cell Adh. Migr.* **7**, 90-100. doi:10.4161/cam.22236

Vidal, F., Baudoin, C., Miquel, C., Galliano, M. F., Christiano, A. M., Uitto, J., Ortonne, J. P. and Meneguzzi, G. (1995). Cloning of the laminin alpha 3 chain gene (LAMA3) and identification of a homozygous deletion in a patient with Herlitz junctional epidermolysis bullosa. *Genomics* **30**, 273-280. doi:10.1006/geno.1995.9877

Zenker, M., Aigner, T., Wendler, O., Tralau, T., Müntefering, H., Fenski, R., Pitz, S., Schumacher, V., Royer-Pokora, B., Wühl, E. et al. (2004). Human laminin beta2 deficiency causes congenital nephrosis with mesangial sclerosis and distinct eye abnormalities. *Hum. Mol. Genet.* **13**, 2625-2632. doi:10.1093/hmg/ddh284

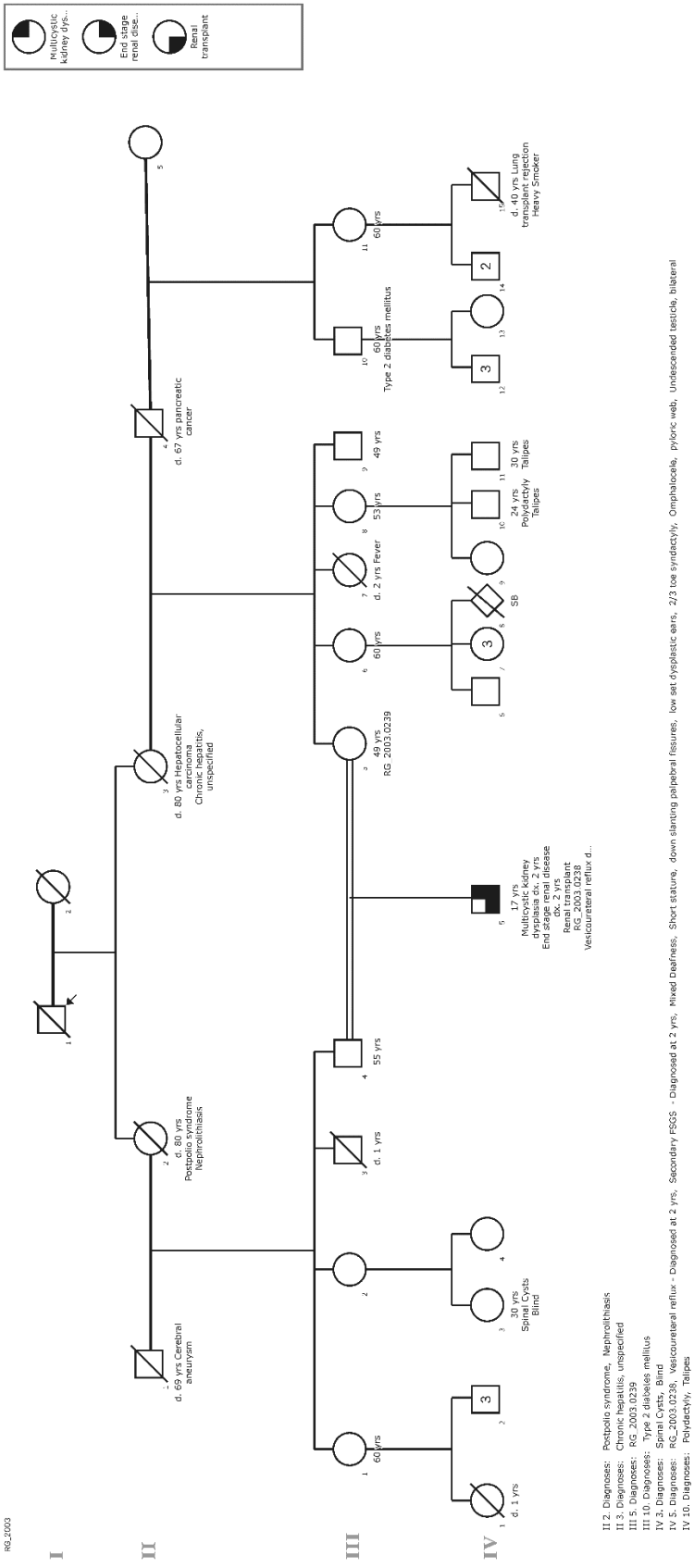

Figure S1 – Pedigree of the affected proband

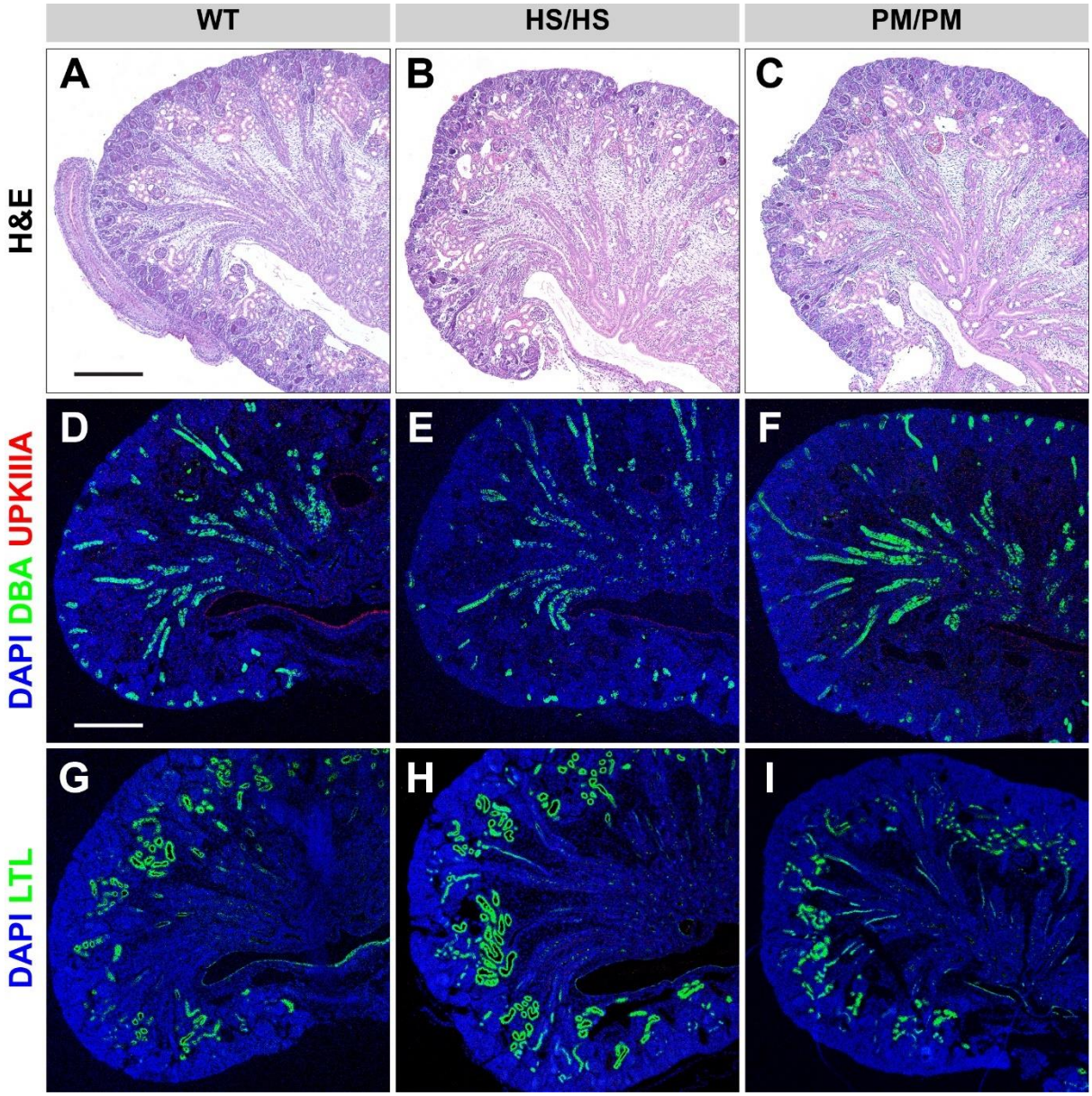

Figure S2

Patterning of the collecting duct and nephron segments in mice of different genotypes indicate that fetal kidney development is unaffected by the introduction of CRISPR mediated changes in *Lama5*.

Table S1: Homozygous candidate variants

CHROM:POS:REF:ALT	HGVS	Symbol	Impact	CADD[1]	GnomAD	
					Popmax AF[2]	Hom Alt count[3]
4:71394470:G:A	NM_212557.4:c.325G>A (p.Ala109Thr)	AMTN	Missense	22.7	0.00609089	3
6:126236629:G:A	NM_181782.5:c.2244+3G>A	NCOA7	Splice Region	14.2	0.00137387	0
9:71836037:C:T	NM_001170416.2:c.670C>T (p.Arg224Trp)	TJP2	Missense	23.0	0.000225225	0
9:79322098:T:C	NM_015225.3:c.5092A>G (p.Ile1698Val)	PRUNE2	Missense	0.0	3.27E-05	0
9:84205855:C:T	NM_005077.5:c.1694G>A (p.Arg565His)	TLE1	Missense	31.0	8.79E-06	0
12:25261759:T:TAAAAAAAAAAAAAA	NM_018272.5:c.1894-16_1894-3dupTTTTTTTTTTTTTT	CASC1	Splice Region	12.6	n.f.	n.f.
12:108988326:C:CAAAAAAAAAA	NM_181724.3:c.-14-2163_-14-2154dupTTTTTTTTT	TMEM119	Splice Region	0.6	n.f.	n.f.
13:32367033:C:G	NM_130806.5:c.1594C>G (p.Arg532Gly)	RXFP2	Missense	23.0	0.00155521	0
13:45150143:G:C	NM_183422.4:c.68C>G (p.Ala23Gly)	TSC22D1	Missense	26.0	n.f.	n.f.
13:46124056:T:C	NM_182542.3:c.1618A>G (p.Thr540Ala)	ERICH6B	Missense	25.1	0.00530845	8
14:73996946:C:T	NM_203309.2:c.-72-7018G>A	HEATR4	Splice Region	0.4	0.00673563	0
16:47005573:T:TAAAAAAAA	NM_005880.4:c.139-97_139-90dupTTTTTTTT	DNAJA2	Splice Region	3.9	n.f.	n.f.
19:9075370:T:C	NM_024690.2:c.12076A>G (p.Thr4026Ala)	MUC16	Missense	0.0	0.00911944	8
19:12991919:G:C	NM_001375.3:c.134C>G (p.Ala45Gly)	DNASE2	Missense	9.1	0.00789852	5
19:17445470:C:T	NM_020959.3:c.10G>A (p.Ala4Thr)	ANO8	Missense	11.6	0.00865209	9
20:5528409:G:C	NM_019593.5:c.1917C>G (p.Ser639Arg)	GPCPD1	Missense	22.2	n.f.	n.f.
20:18295980:C:T	NM_001083330.4:c.482C>T (p.Thr161Ile)	ZNF133	Missense	11.8	0.00466805	0
20:60926966:C:A	NM_005560.6:c.857G>T (p.Arg286Leu)	LAMA5	Missense	32.0	n.f.	n.f.
22:47164079:G:A	NM_014346.5:c.62+5334G>A	TBC1D22A	Splice Region	8.7	0.00331169	0

1) CADD *In silico* damage prediction score. Scores > 20 are predicted to be damaging. CADD v1.6 (Rentzsch P et al, NAR, 2019).
2) Maximum population allele frequency observed in gnomAD v2.1.1 database.
3) Number of individuals in gnomAD v2.1.1 database homozygous for the variant.

Table contains all variants homozygous variants identified in the proband that meet all of the following criteria:

- PASS GATK VQSR quality filters.
- Homozygous in the proband and heterozygous in the probands mother.
- Maximum population Allele frequency < 0.01 (gnomAD v2.1.1).
- Fewer than 20 homozygous individuals observed in gnomAD v2.1.1.
- Predicted to alter the protein coding sequence of one or more gencode tsl1 transcripts.

Reference
Rentzsch P, Witten D, Cooper GM, Shendure J, Kircher M. CADD: predicting the deleteriousness of variants throughout the human genome. Nucleic Acids Res. 2019 Jan 8;47(D1):D886-D894.